NASA TECHNICAL NOTE

NASA TN D-3016

NASA TN D-3016

INVESTIGATION OF EXHAUST BACKFLOW FROM A SIMULATED CLUSTER OF THREE WIDE-SPACED ROCKET NOZZLES IN A NEAR-SPACE ENVIRONMENT

by James M. Cubbage

Langley Research Center
Langley Station, Hampton, Va.

NATIONAL AERONAUTICS AND SPACE ADMINISTRATION • WASHINGTON, D. C. • SEPTEMBER 1965

INVESTIGATION OF EXHAUST BACKFLOW FROM A SIMULATED CLUSTER OF THREE WIDE-SPACED ROCKET NOZZLES IN A NEAR-SPACE ENVIRONMENT

By James M. Cubbage

Langley Research Center
Langley Station, Hampton, Va.

NATIONAL AERONAUTICS AND SPACE ADMINISTRATION

For sale by the Clearinghouse for Federal Scientific and Technical Information
Springfield, Virginia 22151 – Price $3.00

INVESTIGATION OF EXHAUST BACKFLOW FROM A SIMULATED CLUSTER OF THREE WIDE-SPACED ROCKET NOZZLES IN A NEAR-SPACE ENVIRONMENT

By James M. Cubbage
Langley Research Center

SUMMARY

A limited experimental investigation has been conducted to confirm the existence of exhaust backflow from a cluster of three widely spaced nozzles operating in a near-space environment and to determine pressures and heat-transfer coefficients in the region washed by the backflow. Experiments were conducted in a 61-foot-diameter vacuum sphere using a single solid-propellant rocket motor and a reflection plate. The reflection plate was used to simulate the interference planes that would normally exist for a cluster of three nozzles. Data were obtained for nozzle spacings of 8.02 and 17.05 nozzle exit diameters for pressures which simulated a nominal altitude range of 3.2×10^5 to 1.8×10^5 feet. The pressure data indicated that the backflow was supersonic for several nozzle exit diameters ahead (upstream) of the nozzle exit plane and that the flow over small-diameter thermocouples in this region was in the free-molecule region. Average heat-transfer coefficients obtained for small-diameter cylinders (thermocouples) in this region were on the order of 1×10^{-4} Btu/sq ft-sec-$^{\circ}$R.

INTRODUCTION

The grouping of several nozzles in a cluster on a rocket-powered vehicle introduces a flow phenomenon that is a direct result of exhaust plume expansion. This flow phenomenon is generally referred to as exhaust backflow and occurs when the expanding exhaust plumes from adjacent nozzles impinge upon each other and create a shock pattern and attendant pressure gradient that cannot be negotiated by a portion of the flow in the plume boundaries. Consequently, this portion of the exhaust flow turns and flows in a direction opposite to the main nozzle flow. The high stagnation temperature of this backflow imposes a convective heat load on the vehicle base and nearby components and, unless suitable protection is provided for these items, destructive damage to the vehicle may result. Therefore, a number of investigations have been conducted (refs. 1 to 6, for example) to determine base heating rates for various configurations over a range of altitudes. Much of this work was experimental, as the many factors involved make analytical study very difficult, and is characterized by nozzle

spacings less than the nozzle exit diameter and ambient pressures which simulate a maximum altitude of about 1.5×10^5 feet.

In space, where the exhaust plume expansion is a maximum, interference between exhaust plumes from a cluster of nozzles may occur even with large separation between adjacent nozzles. The open-framework type of construction used for certain types of space vehicles would expose certain components to exhaust backflow from clusters of propulsive or control rocket motors. An example of this is the Surveyor spacecraft where the three vernier control rockets have a spacing of about 11.8 nozzle exit diameters and a base, in the normal sense, is absent. Even with this large nozzle spacing the exhaust plumes will impinge upon each other only a short distance from the nozzles and the expected backflow would wash components and structure located behind the control rockets. Although the heat transferred to these items from any backflowing exhaust gases should be small because of the low density of the backflow, it may become larger than desired if the backflow velocity is high or if backflow chokes escape passages and thus creates regions of relatively high pressure. In addition, the backflow may tarnish highly polished surfaces and thus increase the solar radiative heat flux to these surfaces.

The exploratory investigation reported herein was undertaken to confirm the existence of exhaust backflow for large nozzle spacings in a near-space environment and to investigate the pressures and heat transfer in the region washed by the unrestricted backflow. Tests were conducted in a 61-foot-diameter vacuum sphere using a single solid-propellant rocket motor and a reflection plate. The reflection plate was used to simulate the interference planes that would normally exist for a cluster of three nozzles. Pressures and heat-transfer coefficients in the backflow region were determined for nozzle spacing ratios (ratio of distance between nozzle exit diameters to the nozzle exit diameter) of 8.02 and 17.05 over a nominal altitude range of 3.2×10^5 to 1.8×10^5 feet.

SYMBOLS

A	area, $\frac{\pi d}{12}L$ for thermocouples and $\frac{\pi}{4}\left(\frac{d}{12}\right)^2$ for calorimeters, sq ft
c	specific heat, Btu/lb-$^\circ$F
C_t	shortest distance between inside edges of adjacent nozzles measured in plane of nozzle exits, in. (see fig. 1)
$\frac{C_t}{d_e}$	nozzle spacing ratio
d	diameter of thermocouple wire or diameter of calorimeter disk, in.
h	convective heat-transfer coefficient, $\frac{q/A}{T_t - T}$, Btu/sq ft-sec-$^\circ$F
L	length of thermocouple wire loop, ft

M	backflow Mach number
$N_{Nu,o}$	Nusselt number with thermal conductivity determined at stagnation temperature of backflow
p	pressure, lb/sq in. absolute
$\frac{p_{t,c}}{p_\infty}$	nozzle total-pressure ratio
$\frac{p_s}{p_\infty}$	reflection-plate static-pressure ratio
$\frac{p_t}{p_\infty}$	backflow total-pressure ratio
q	heating rate, Btu/sec
$\frac{q}{A}$	heat flux, Btu/sq ft-sec
R	gas constant, ft/$^\circ$F
N_{Re}	backflow unit Reynolds number, 1/ft
$N_{Re,o}$	Reynolds number used in correlating heat-transfer data, based on diameter of thermocouple wire with viscosity of backflow evaluated at stagnation conditions and density at free-stream conditions
$N_{Re,T}$	thermocouple Reynolds number based on wire diameter
t	time, sec
T	temperature, $^\circ$F
T1, T2, etc.	thermocouple or calorimeter position designation on reflection plate (see fig. 3(b))
w	specific weight, lb/cu ft
W	weight, lb
y	distance perpendicular to surface of reflection plate, in.
α	angle between tangent to exhaust boundary at nozzle exit and nozzle center line, deg
β	angle between tangent to exhaust boundary and reflection plate at the point of intersection of exhaust boundary and reflection plate, deg

γ	ratio of specific heats

Subscripts:

c	combustion chamber
e	nozzle exit
C	heat meter or calorimeter
s	reflection-plate surface
t	total
T	thermocouple
∞	ambient or sphere conditions

APPARATUS AND METHODS

Facility

The investigation reported herein was conducted in the Langley 61-foot-diameter vacuum sphere. The sphere pressure before firing of the rocket motor was approximately 3×10^{-4} millimeters of mercury for all tests and the post-fire pressure was approximately 0.26 millimeter of mercury. The altitude range corresponding to these pressures was about 3.2×10^5 to 1.8×10^5 feet. Initial evacuation of the sphere to a few millimeters of mercury was accomplished by positive displacement type of pumps and final pump-down by diffusion pumps. A McLeod gage was used to determine the sphere pressure before firing of the rocket motor. Post-fire sphere pressure was measured by an electronic vacuum gage.

Model

To eliminate the problem of obtaining equal performance and simultaneous ignition of three rocket motors and to reduce the sphere pressure rise to a minimum, a reflection plate was placed adjacent to a single rocket motor to simulate the interference planes that would normally exist for a cluster of three nozzles. This procedure is illustrated in figure 1. The 1/4-inch-thick steel reflection plate was supported 10 feet above the floor in the sphere by a steel framework (fig. 2). The rocket motor and its combination holder and thrust measurement transducer (load cell) were supported adjacent to the plate by a section of steel pipe. The center of the nozzle was located 6 inches $\left(\frac{C_t}{d_e} = 8.02\right)$ and 12 inches $\left(\frac{C_t}{d_e} = 17.05\right)$ from the plate being measured as shown in figure 2.

The polyurethane propellant rocket motor had a nominal thrust of 100 pounds and a useful burning time of about 4 seconds. The combustion-chamber pressure and temperature were approximately 650 lb/sq in. abs and 4800 °F, respectively. The conical nozzle was an integral part of the motor casing and had a half-angle expansion of 30 with a nominal throat diameter of 0.3 inch and an exit diameter of 1.33 inches. For these dimensions and a ratio of specific heats of 1.22, the exit Mach number was 3.83. A conical nozzle was used so that the angle through which the exhaust flow turned at the nozzle exit for the conditions of this experiment would more nearly approximate that which would occur in space for a contoured nozzle. (See ref. 7.)

Instrumentation

The location and designation of the 16 thermocouple or calorimeter mounting holes and the six 0.060-inch-diameter static-pressure orifices on the reflection plate are shown in the drawings presented as figure 3. Since the height of the thermocouples and calorimeters above the reflection plate and the location of the total-pressure probe was varied for each nozzle spacing ratio, configuration numbers were assigned to each motor firing. These configuration numbers and the corresponding thermocouple and calorimeter heights and probe locations are listed in the table of figure 3(b). The manner in which the thermocouples and calorimeters were installed in the reflection plate and the height designated is shown in the sketch of figure 3(a).

Pressures.- In addition to the six static pressures measured on the plate, the sphere pressure, rocket-motor combustion-chamber pressure, and the total pressure of the exhaust backflow were also recorded. The plate static pressures and the backflow total pressure were measured with 0.1 lb/sq in. differential, inductance-type transducers calibrated for a pressure range equivalent to 2 inches of water. These transducers were connected to the pressure orifices by 2-inch-long, 1/8-inch inside diameter tubing. The sphere pressure was measured with a similar type of transducer calibrated for a pressure range equivalent to 1 inch of water. This transducer was referenced to a small pressure chamber that was maintained at the pressure existing in the sphere prior to motor ignition. All other pressures were referenced to the sphere pressure. The rocket-motor combustion-chamber pressure was measured by a transducer with a range of 1000 pounds per square inch tapped into the end of the combustion chamber.

Thermocouples and calorimeters.- All thermocouples used in this investigation were chromel-alumel. Two wire sizes, 0.005 inch and 0.010 inch in diameter, were chosen as a compromise between anticipated response and durability requirements. The larger wire thermocouples were generally used in locations close to the nozzle exit.

Drawings showing the manner in which the thermocouple probes and calorimeters were constructed are presented as figure 4. The chromel and alumel wires for the thermocouple probes were joined by first flattening the end of the two wires slightly and then spot-welding together. The junction thus formed was then dressed with a file to roughly the same diameter as the wire. The thermocouple wires were then passed through a 2-inch length of two-hole ceramic

tubing and spliced to larger gage chromel and alumel wires. This assembly was then slipped into a 3-inch length of 3/16-inch outside diameter stainless steel tubing and sealed at both ends with ceramic cement. Construction of the calorimeters was similar with the exception that the formation of the thermocouple junction and its contact with the bottom surface of the copper disk was accomplished with one spot-welding operation. The weight of each copper disk was determined by means of a chemical balance before attachment of the thermocouple wires. Tables listing the property parameter $\frac{d}{12}\frac{wc}{4}$ and $\frac{Wc}{A}$ for the individual thermocouples and calorimeters and their locations on the reflection plate for the model configurations investigated are presented in figure 5. Also shown in this figure are enlarged silhouettes of two typical thermocouple junctions.

Data Reduction and Accuracy

All data obtained during a test run were recorded with recording oscillographs. These records were then transcribed manually into punch-card form and machine processed. Data readout was in the form of absolute and differential pressures and temperatures.

Experimental heat flux to the disk calorimeters and thermocouples was calculated from the temperature-time histories by using the following equation:

$$\frac{q}{A} = k\frac{\Delta T}{\Delta t} \tag{1}$$

where $k = \frac{d}{12}\frac{wc}{4}$ for the thermocouples and $k = \frac{Wc}{A}$ for the calorimeters. (For the thermocouples, A was taken as the entire surface area of the exposed thermocouple wire.) The rate of change of temperature with time was obtained manually from the temperature-time plots; this procedure introduces a random error in the computed heating rates. The specific heat of the thermocouples was taken as the arithmetical average between the specific heats for the chromel and alumel wires.

The use of equation (1) involves the following assumptions: (1) heat loss due to radiation is negligible; (2) heat loss due to conduction through the thermocouple lead wires is negligible; (3) the thermal conductivity of the disk calorimeters and thermocouples is such that the temperature difference through the calorimeter disk and through the exposed thermocouple wire is negligible; and (4) the heat-transfer coefficient is invariant with temperature. For the present investigation the error in the measured heat flux introduced by the first two assumptions was calculated to total about 6 percent (less than 2 percent by radiation and about 4 percent by conduction) for the time period of 1.2 seconds after motor ignition for which heat-transfer coefficients are presented. These losses were calculated for the thermocouple having the highest temperature rise in this time period. This error was considered to be small for this investigation; therefore, the heat-flux calculations were not corrected for these losses.

Another possible source of error in the temperature data is the heat flux due to radiation from the exhaust plume to the thermocouples. This error was found to be negligible from a preliminary test run in which the exhaust plume barely impinged upon the reflection plate (essentially no backflow). The temperature rise experienced by the thermocouples for this run was essentially the same as the temperature rise of the sphere thermocouple which could not see the exhaust plume.

Heat-transfer coefficients were obtained from a modified definition of the convective heat-transfer coefficient

$$h = \frac{q/A}{T_t - T} \tag{2}$$

where the usual recovery or adiabatic wall temperature has been replaced by a total temperature. The adiabatic wall temperature was impractical to evaluate in the present investigation and, since it is not readily available in most cases, the heat-transfer coefficient was based on the total temperature of the backflow. This total temperature was, in turn, assumed to be equal to the rocket-motor combustion-chamber temperature (4800° F).

The accuracy of the temperature and pressure measurements is estimated to be as follows:

Temperature, $^\circ$F	±3
Combustion-chamber pressure, lb/sq in.	±10
Static pressure, lb/sq in.	±0.001
Sphere pressure, lb/sq in.	±0.0004

For the reflection-plate static pressures and the sphere pressure, the error listed is the maximum estimated to occur when only the accuracy of the pressure transducer and the accuracy in reading the oscillograph traces are considered. The total-pressure probe readings were subject to an unknown error because of possible misalinement with the flow. The probe was alined parallel with the reflection-plate center line for all configurations.

RESULTS AND DISCUSSION

Pressure Data

Sphere pressure and rocket-motor performance.- The sphere pressure, rocket-motor combustion-chamber pressure, and rocket-motor thrust measured during the several rocket-motor firings of this investigation are presented in figures 6 and 7. The geometric altitude corresponding to the sphere pressure scale in figure 6 is the right-hand ordinate in this figure. The useful burning time of the rocket motor was about 4 seconds except in the case of the motor of configuration II (fig. 7). For this configuration the useful burning time was about 3.5 seconds as indicated by the rapid decrease in combustion-chamber pressure at this time value. The curves in figure 7 between $t = 0$ and $t = 0.2$ have been arbitrarily faired through the data scatter obtained in this time period.

It will be noted in figures 6 and 7 that there is a lack of consistency between the sets of curves. For example, the rocket motor with the highest combustion-chamber pressure did not have the highest value of thrust and the motor with the highest thrust did not yield the greater sphere pressure. It is felt that the main reasons for this inconsistency are the probable differences in throat areas and combustion temperatures of the propellants between the several nozzles used in this investigation. A graphite insert was used for the throat of the nozzle and there was no strict dimensional control over these inserts.

Nozzle pressure ratio and exhaust boundary.- The variation of nozzle total-pressure ratio with time presented in figure 8 was computed by using values of $p_{t,c}$ and p_∞ midway between the maximum and minimum values at a given value of time t in figures 6 and 7. The approximate nozzle static-pressure ratio (ratio of nozzle exit pressure to the sphere pressure) for the same conditions may be obtained from figure 8 by using the nominal value $\frac{p_e}{p_{t,c}} = 0.005$ and the plotted values of $\frac{p_{t,c}}{p_\infty}$.

The angle β at which the computed exhaust boundary strikes the reflection plate for the two spacing ratios is given in figure 8 for two nozzle pressure ratios. The exhaust boundaries were computed by the method of reference 7 by using the median nozzle pressure ratio curve of figure 8, a ratio of specific heats of 1.22, and the nozzle dimensions.

Reflection-plate static pressures.- Static pressures measured on the reflection plate are presented in the form of a ratio to the sphere pressure for several periods of time after motor ignition in figures 9 and 10. Figure 9 presents this ratio for a line perpendicular to the vertical center line (bend) of the reflection plate and located 8 inches ahead or upstream of the nozzle exit. Similarly, figure 10 shows the static pressure distributions obtained along a line parallel to the bend in the reflection plate. This line was offset about 1 inch from the bend. The curves of figures 9 and 10 were obtained by first plotting the absolute pressure time history for each orifice and fairing a smooth curve through these data points. The ratio p/p_∞ was then computed from these faired curves and the corresponding sphere pressure data. The pressure distributions were then obtained from these plots of p/p_∞ against time for the indicated times in figures 9 and 10 by assuming flow symmetry about the plate center line; that is, pressure orifice p_2 was transposed to a location between p_3 and p_4. The pressure data obtained for $t < 1.0$ second suffers from lack of accuracy because of the low pressures generally obtained in this time period. In some cases negative absolute pressures were indicated in this time period. For these cases the curve for pressure plotted against time was faired to zero pressure at $t = 0$.

If, in figure 9, only that portion of the pressure-distribution curves between the plate center line and 8 inches from the center line is considered for $t > 1.0$, a region of high pressure is noted between 5 and 7 inches from the plate center line for both spacing ratios. The pressures measured at the

outer edge of the plate for the larger spacing ratio (fig. 9(b)) appear to be abnormally high when compared with the other measured plate pressures. The pressure distributions obtained parallel to the plate center line for $\frac{C_t}{d_e} = 8.02$ (fig. 10(a)) show a rapid rise in pressure from the exit plane to the line of orifices of figure 9 (8 inches upstream from the nozzle exit plane) for $t > 0.4$. However, this rise in pressure occurs only at $t = 0.4$ for the larger spacing configuration of figure 10(b). For other values of t, the pressure increases gradually as the distance increases. Also to be noted in figures 9 and 10 is the increase in p_s/p_∞ for a given orifice with time. Further discussion of these observations will be made in the section entitled "Flow Model."

Backflow total pressures.- The total pressure of the exhaust backflow was measured at three locations on the reflection plate for the smaller nozzle spacing configuration and at one location for the larger spacing configuration. (See fig. 3(b).) Total-pressure time histories for these locations are presented in figure 11 as a ratio of the sphere pressure. Also presented in this figure are reflection-plate static-pressure-ratio time histories corresponding to the total-pressure time histories. Static pressures shown for configurations I and II were obtained for the probe location from reflection-plate static-pressure contours. For configurations III and IV, however, it was necessary to use the static pressures from an orifice located some distance from the probe (see figs. 11(c) and 11(d)); thus, the pressure at this orifice may or may not be indicative of the static pressure at the probe location. It will be noted that the probe total-pressure ratio eventually becomes less than the plate static-pressure ratio for all configurations except configuration III. This difference would indicate that the backflow has ceased and the probe is subject to flow from the opposite direction.

Backflow Mach numbers and unit Reynolds number.- The interpretation of measured total pressures in a rarefied gas is complicated by viscous forces which become appreciable compared with the inertia or pressure forces in the flow; that is, the total pressure is related to a Reynolds number in addition to the Mach number and static pressure. A discussion of the analytical work of reference 8 in reference 9 shows that, for the total-pressure probe considered in reference 9, the difference between a measured total pressure and the total pressure determined from the Rayleigh pitot formula for known values of Mach number and static pressure is large at low supersonic Mach numbers. In reference 9, the measured value exceeded the computed value by 60 percent at Mach 1.5. At hypersonic Mach numbers the difference approaches a near constant value of 11 percent.

The analysis of reference 8 was used in the calculation of the backflow Mach number from the pressure data of figure 11. The resulting Mach number variation with time for these data is presented in figure 12. It will be noted here that there is a considerable variation in Mach number with time as well as laterally across the plate for a given time. (Configurations I, II, and III are for $\frac{C_t}{d_e} = 8.02$.)

In order to compute the unit Reynolds number of the backflow, it was necessary to evaluate the viscosity of the exhaust gas. The composition of the exhaust gas mixture and its gas constant R were known from data supplied by the propellant manufacturer. The viscosities of the individual gases were obtained from reference 10 and the viscosity of the mixture was then approximated by combining the percent by weight of the viscosity of the individual gases. The use of a more accurate method of determining the viscosity of the mixture, such as the procedure of reference 11, involves further assumptions that did not appear to be justified from the data available.

The results of the Reynolds number calculations are presented in the lower portion of figure 12. These Reynolds number time histories correspond to the Mach number time histories shown in the upper portion of figure 12. The unit Reynolds number is seen to be of the order of magnitude of 1 so that a Reynolds number based on the diameter of the thermocouple wire is extremely small. Calculation of the Knudsen number K from these values of Mach number and Reynolds number by the relationship

$$K = 1.26\sqrt{\gamma}\,\frac{M}{N_{Re,T}}$$

yielded a minimum value of K of about 38. Thus, the data obtained for the thermocouples were well into the free-molecule flow region. (See ref. 13.)

Temperature Data

Sphere gas temperature.- Temperature time histories obtained for the sphere thermocouple for the five configurations of this investigation are presented in figure 13. This thermocouple was located behind the reflection plate and could not "see" the rocket motor or the exhaust plume. The temperature rise indicated by the sphere thermocouple in figure 13 for a given configuration results from the hot exhaust gases and the compression of these gases within the sphere during the burning time of the rocket motor. Any of the plate thermocouples not subject to the exhaust backflow should also register this temperature rise. It will be noted that the sphere gas temperature rise for configurations II and V was somewhat lower than the temperature rise for the other three configurations.

Position T1 thermocouple.- The temperature time histories for the thermocouple in position T1 (see fig. 3(b)) for the five configurations are presented in figure 14. These time histories are characterized by an initial, rapid rise in temperature followed by a leveling off or slight decrease in temperature. The smaller nozzle spacing configurations (configurations I, II, and III) exhibit the greatest overall temperature rise, this rise being two to three times as great as that for the $\frac{C_t}{d_e} = 17.05$ configurations (configurations IV and V). Since this thermocouple was located in the plane of the nozzle exit, it was subject to direct exhaust-gas impingement (especially so for the smaller nozzle spacing) and greater radiation effects from the exhaust

gases. Direct exhaust-gas impingement during the early moments after motor ignition would account for the rapid temperature rise noted in this time period. The decrease in the rate of temperature rise or the leveling off of the temperature between 1.6 and 2.4 seconds, depending upon the configuration, is thought to be due to changing flow conditions as the sphere pressure increases. That is, the thermocouple is subject initially to direct impingement but as the sphere pressure increases, the plume boundary strikes the reflection plate further downstream and the thermocouple comes under the influence of the backflow. The differences in thermocouple response between the configurations for a given nozzle spacing can be attributed to the differences in height of the thermocouple above the reflection plate. The zero thermocouple height of configurations II and III may place the thermocouple in closer proximity to any high-pressure region on the plate because of plume impingement than the 1-inch height of configuration I. For the larger nozzle spacing, however, by assuming little or no direct impingement, the zero-height thermocouple of configuration V would be subject to backflow that has been cooled by passage over the reflection plate.

In view of the uncertainty as to the flow conditions existing for thermocouple T1, these data will not be discussed further insofar as backflow heat-transfer coefficients are concerned. However, as a matter of interest, the order to magnitude of h for configurations II and III is about 1×10^{-3} $Btu/ft^2\text{-}sec\text{-}^oF$.

Plate thermocouples and disk calorimeters.- Temperature time histories of the thermocouples and disk calorimeters located in positions T2 to T16 are presented in figures 15 to 19 for the five configurations. The temperature time history of the thermocouple used to measure the sphere gas temperature is also presented in each figure for comparison purposes.

Of general interest in figures 15 to 19 is the response of the plate thermocouples relative to that for the sphere thermocouple. It will be noted that only for configuration I $\left(\frac{c_t}{d_e} = 8.04, \quad y_T = 1 \text{ inch}\right)$ is the temperature rise of the plate thermocouples generally greater than that for the sphere thermocouple over the burning time of the rocket motor. For configurations II and III $\left(y_T = 0\right)$ at this nozzle spacing, the temperature rise of the plate thermocouples is generally less than that for the sphere thermocouple except near the exit plane of the nozzle. This reduction in temperature rise for these configurations is attributed to cooling effects of the reflection plate on the backflow next to the plate. The distance perpendicular to the plate that this cooling effect (or thermal gradient) would extend would increase as the distance upstream from the nozzle exit increased. Therefore, it is reasonable to expect that even those thermocouples that were extended 1 inch above the plate surface (configurations I and IV) and located some distance upstream of the nozzle may have been adversely influenced by the presence of the plate. At the larger nozzle spacing the plate thermocouples exhibit an initial temperature rise that is generally greater than that for the sphere thermocouple. However, a rather abrupt change in the temperature rise occurs between about 1.5 to 2.0 seconds after motor ignition for most of the thermocouples and the temperature of these

thermocouples thereafter increases at a much slower rate or shows a decrease in temperature. This temperature response of the plate thermocouples suggests a significant change in the backflow pattern or complete cessation of the backflow rather than attainment of equilibrium temperature by the thermocouples.

The temperature rise of the disk calorimeters noted in figures 15 to 19 is, of course, less than that for the thermocouples because of the greater heat capacity of the calorimeters. In figures 17(a) and 18(a) it will be noted that a calorimeter was mounted perpendicular to the backflow at position T10 for configuration III and at position T5 for configuration IV.

Validity of nozzle cluster simulation method.- The significance of the pressure and temperature data discussed in the foregoing paragraphs is dependent upon whether the reflection plate was a valid representation of the planes of interference that would normally occur for a cluster of three nozzles. Data and schlieren photographs from reference 12 and an unpublished source yielded strong evidence that the reflection plate would be a valid representation of these interference planes. Part of this evidence is shown in the schlieren photographs of figure 20. The top photograph in this figure is from reference 12 and depicts a sonic nozzle operating at a static-pressure ratio of about 5×10^4. The bottom photograph is a schlieren view of a cluster of four sonic nozzles operating at a static pressure ratio of about 20. It will be noted in this figure that the shock produced at the impingement point of the exhaust flows from two adjacent nozzles (bottom photograph) is very similar to the one produced by the flow from a single nozzle impinging upon a flat plate (top photograph). Base-pressure measurements on the four-nozzle cluster in figure 20 show that the presence of a reflection plate to simulate the flow from two of the nozzles had no significant effect on base pressures for nozzle spacings greater than $\frac{C_t}{d_e} = 0.75$. At lesser spacings the boundary layer on the plate caused an effective nozzle spacing less than the geometric spacing.

It would appear from the foregoing that the use of a reflection plate to simulate a nozzle cluster was a valid experimental procedure for the purpose of this investigation. However, it should be pointed out that it is possible to conceive of circumstances where erroneous data may result from use of this method. For example, it can be postulated that in a space environment the mean free path of the molecules in the outermost portions of the exhaust plumes may be so large that the plumes would initially intermingle without mutual interference. In this case, the backflow would not originate along the lines of initial plume contact but from a higher pressure region within the merged plumes where formation of interference shocks would be possible. For this situation the approaching streamlines from the individual plumes would meet at a shallower angle, and thus reduce the quantity of backflow or, at the extreme, eliminate it entirely. Therefore, in this circumstance the reflection plate would produce a greater amount of backflow than would occur from the actual cluster of nozzles being simulated or, if viewed from the standpoint of nozzle spacing, the reflection plate would create an effective spacing ratio smaller than the geometric one. Since it is not known whether this or any other similar circumstance existed for the present investigation, the data are presented on the basis that the reflection plate was a valid experimental procedure for the purpose intended.

Flow Model

The supersonic velocities measured in the backflow of this investigation support the results of reference 6 wherein data are presented that indicate that the backflow is supersonic a short distance from the common impingement point of the nozzle plumes. Therefore, for the balance of this discussion it is assumed that the backflow becomes supersonic at or very near the line of impingement of the exhaust plume on the reflection plate. With this in mind and consideration of the data presented and the post-fire photograph of the reflection plate in figure 21(a), a possible explanation of the behavior of the backflow in the present investigation can be set forth. A factor which enters into the explanation is the circulation of the gases within the sphere induced by the rocket exhaust flow. This circulating flow and the other factors under discussion are shown in the drawing of figure 21(b). In this figure the supporting framework for the reflection plate is not shown and only the top portion of the rocket motor case is depicted.

In figure 21(a) a sharply defined semicircular area on the reflection plate will be noted wherein the dust from the rocket grain deposited on the plate is less than that outside this area. The region in which the dust "ring" crosses the line of static-pressure orifices coincides with the high-pressure area noted in figure 9(a). This condition suggests that the dust ring (also shown in fig. 21(b)) represents a region of high pressure relative to the sphere pressure and that the increase in pressure is due to a sudden decrease in velocity of the backflow. The latter deduction follows from the lack of dust deposit in a region of known supersonic flow and the heavy deposit in the area surrounding this region. The question arises here as to whether the dust ring represents the interface between the induced flow and the backflow or whether it represents a deceleration of the backflow to subsonic speeds by a shock such as would occur for overexpanded flow in a nozzle and the interface occurs beyond the dust ring as shown in figure 21(b). The latter supposition is felt to be the case here as two of the three calorimeters (T8 and T9) located just beyond the dust ring show heating rates comparable to those applied to the thermocouples within the area enclosed by the dust ring. (See fig. 22.) Thermocouples located further beyond the dust ring on the lower portion of the plate, positions T11 to T16, show an overall temperature increase that is not much greater or somewhat less than that for the sphere thermocouple (fig. 16(b)). The heating rates for these thermocouples shown in figure 22 are larger than the rate for the sphere thermocouple initially but show a sudden decrease to values about equal to or less than the sphere thermocouple rate soon after motor ignition. This decrease suggests that the induced flow becomes predominant in this region of the plate as shown in figure 21(b) soon after motor ignition and the less than sphere thermocouple heating rates result from cooling of the induced flow as it passes over the sphere wall and floor before reaching the model. The rather abrupt decrease in the temperature rise of the thermocouples of the larger nozzle spacing configurations (figs. 18 and 19) suggests that the induced flow becomes a dominant fact over much of the reflection plate soon after motor ignition because of the reduced amount of backflow for this spacing ratio. The concept of an interface between the induced flow and backflow leads to the deduction that the interface acts as an effective base which moves closer to the exit as the sphere pressure increases. If this were the case, it could account for the increase in reflection-plate pressures with time noted previously for figures 9 and 10.

Heat-Transfer Coefficients

Heat-transfer-coefficient profiles.- Average heat-transfer-coefficient distributions for small-diameter cylinders (thermocouples) placed in the backflow for the five configurations are shown pictorially in figure 23. These coefficients are an arithmetical average of the values obtained at five time intervals from $t = 0.4$ to $t = 1.2$ seconds. Only the data to 1.2 seconds were used as these data were believed to be free of any induced-flow effects. A time period of 0.4 second after motor ignition was allowed for establishment of the flow. Average heat-transfer coefficients obtained for the disk calorimeters are listed in the upper left corner of figure 23. It will be noted in this figure that only half of the reflection plate is depicted. The line of thermocouples on the other half (line emanating at $22\frac{1}{2}^{\circ}$ with respect to the plate center line from position T1 in fig. 3(a)) has been transposed to the half shown. Although the temperature data for the thermocouple at position T1 were not considered further because of possible direct exhaust-plume impingement, the curves for the distributions have been faired with the knowledge that, in any case, the value of h would be greater at position T1 than at any other location.

The effect of the thermocouple height above the reflection plate on the heat-transfer coefficient is evident in figure 23 by comparing configuration I with configurations II and III and configuration IV with V. For configuration V the heat meters were at $y_C = 1.0$ inch, whereas the thermocouples were at $y_T = 0$. Comparison of configuration II with configuration III gives an indication of the repeatability of the data since these configurations differed only in the locations of the calorimeters and the total-pressure probe. The heat meters mounted perpendicular to the backflow (figs. 23(c) and 23(d)) show expected higher values of average heat-transfer coefficients. For all configurations the coefficients decrease with increasing distance from the exit, the coefficients closest to the exit having a maximum value of about 3×10^{-4} Btu/sq ft-sec-$^{\circ}$R.

Heat-transfer-coefficient correlation.- The average heat-transfer coefficients obtained for the thermocouples at positions T4, T5, and T6 are compared with empirical and theoretical values for cylinders from references 13 and 14 in figure 24. In this figure the heat-transfer coefficient is presented as a Nusselt number variation with Reynolds number with the viscosity and thermal conductivity in these parameters evaluated at stagnation conditions and the density evaluated at free-stream conditions. The values of h used in the calculation of $N_{Nu,o}$ were taken from the profiles of figure 23. It was assumed for the model $\frac{C_t}{d_e} = 8.02$ that the velocities obtained for configurations II and III were applicable to configuration I in order to compute $N_{Re,o}$ for the thermocouple positions listed in this figure. Since the values of h used were based on the backflow total temperature, the values of $N_{Nu,o}$ obtained were somewhat higher than would be the case if h were based on the recovery temperature; that is, in free-molecule flow the recovery or adiabatic wall temperature is

greater than the total temperature. (For the molecular speed ratios $\sqrt{\frac{\gamma}{2}}\,M$ of the present investigation, the recovery factor is about 1.3.)

It is seen in figure 24 that there is disagreement between the experimental values and the work of reference 13. (The curves of this reference have been extended by about an order of magnitude smaller in fig. 24.) For agreement, the experimental values need to be about two orders of magnitude larger in $N_{Re,o}$ or about one order of magnitude smaller in $N_{Nu,o}$. Extrapolation of the data of reference 14 to the $N_{Re,o}$ values of the present investigation shows good agreement. However, in view of the amount and the range of the data of reference 13, this agreement appears to be coincidental. It is felt that the primary cause for the disagreement in the data of figure 24 is the value of $N_{Re,o}$. Uncertainty exists as to the correctness of the calculated values of this parameter because of the number of assumptions and corrections involved. As suggested in reference 13, the static pressures as well as the total pressures may be subject to errors due to viscous effects. In any case, however, large changes in the static pressure or Mach number would be required to increase $N_{Re,o}$ to the magnitude required for agreement with the data of reference 13.

CONCLUDING REMARKS

Data obtained from an exploratory investigation of exhaust backflow resulting from the mutual interference of exhaust gases from a simulated cluster of three nozzles operating in a near-space environment indicated that backflow was present with spacings of 8.02 and 17.05 nozzle exit diameters between nozzles. Pressure data obtained in the backflow region near the nozzle exit showed that the backflow was supersonic and that the flow over small-diameter thermocouples placed in the backflow region was well into the free-molecule flow region. Average heat-transfer coefficients obtained for small-diameter cylinders (thermocouples) in the backflow region were greater than those predicted by empirical and theoretical methods for cylinders in high-speed rarefied gas flow. This result may have been due, in part, to the inability to calculate an accurate Reynolds number from the pressure data available for the backflow region.

Langley Research Center,
National Aeronautics and Space Administration,
Langley Station, Hampton, Va., May 27, 1965.

REFERENCES

1. Goethert, B. H.: Base Flow Characteristics of Missiles With Cluster-Rocket Exhausts. Paper No. 60-89, Inst. Aeron. Sci., June-July 1960.

2. Musial, Norman T.; and Ward, James J.: Base Flow Characteristics for Several Four-Clustered Rocket Configurations at Mach Numbers From 2.0 to 3.5. NASA TN D-1093, 1961.

3. Allen, John L.: Base-Flow Aerodynamics of a Saturn-Type Booster Stage at Mach Numbers 0.1 to 2.0. NASA TN D-593, 1962.

4. Parker, Joseph R., Jr.; and Gillard, T. J.: An Investigation of Base Heating With a 5.47-Percent Saturn SA-1 Booster Model at Mach Numbers 0.8 and 1.15. AEDC-TN-61-134, U.S. Air Force, Nov. 1961.

5. Dawson, John G., Jr.: An Investigation of Base Heating on a 5.47-Percent-Scale Model Saturn SA-1 Booster Afterbody at Mach Numbers 1.63 and 3.07. AEDC-TDR-62-9, U.S. Air Force, Jan. 1962.

6. Marion, E. D.; Daniels, D. J.; Herstine, G. L.; and Burge, G. W.: Exhaust Reversal From Cluster Nozzles - A New Flow Model. [Preprint] 2706-62, Am. Rocket Soc., Nov. 1962.

7. Vick, Allen R.; Andrews, Earl H., Jr.; Dennard, John S.; and Craidon, Charlotte B.: Comparisons of Experimental Free-Jet Boundaries With Theoretical Results Obtained With the Method of Characteristics. NASA TN D-2327, 1964.

8. Chambre', P. L.; and Schaaf, S. A.: The Theory of the Impact Tube at Low Pressures. J. Aeron. Sci., vol. 15, no. 12, Dec. 1948, pp. 735-737.

9. Kane, E. D., and Maslach, G. J.: Impact-Pressure Interpretation in a Rarefied Gas at Supersonic Speeds. NACA TN 2210, 1950.

10. Brokaw, Richard S.: Alignment Charts for Transport Properties, Viscosity, Thermal Conductivity, and Diffusion Coefficients for Nonpolar Gases and Gas Mixtures at Low Density. NASA TR R-81, 1961.

11. Bromley, L. A.; and Wilke, C. R.: Viscosity Behavior of Gases. Ind. Eng. Chem., vol. 43, no. 7, July 1951, pp. 1641-1648.

12. Vick, Allen R.; and Andrews, Earl H., Jr.: An Experimental Investigation of Highly Underexpanded Free Jets Impinging Upon a Parallel Flat Surface. NASA TN D-2326, 1964.

13. Stalder, Jackson R.; Goodwin, Glen; and Creager, Marcus O.: Heat Transfer to Bodies in a High-Speed Rarefied-Gas Stream. NACA Rep. 1093, 1952. (Supersedes NACA TN 2438.)

14. Kovásznay, Leslie S. G.; and Tôrmarck, Sven I. A.: Heat Loss of Hot Wires in Supersonic Flow. Bumblebee Rep. No. 127, The Johns Hopkins Univ., June 1950.

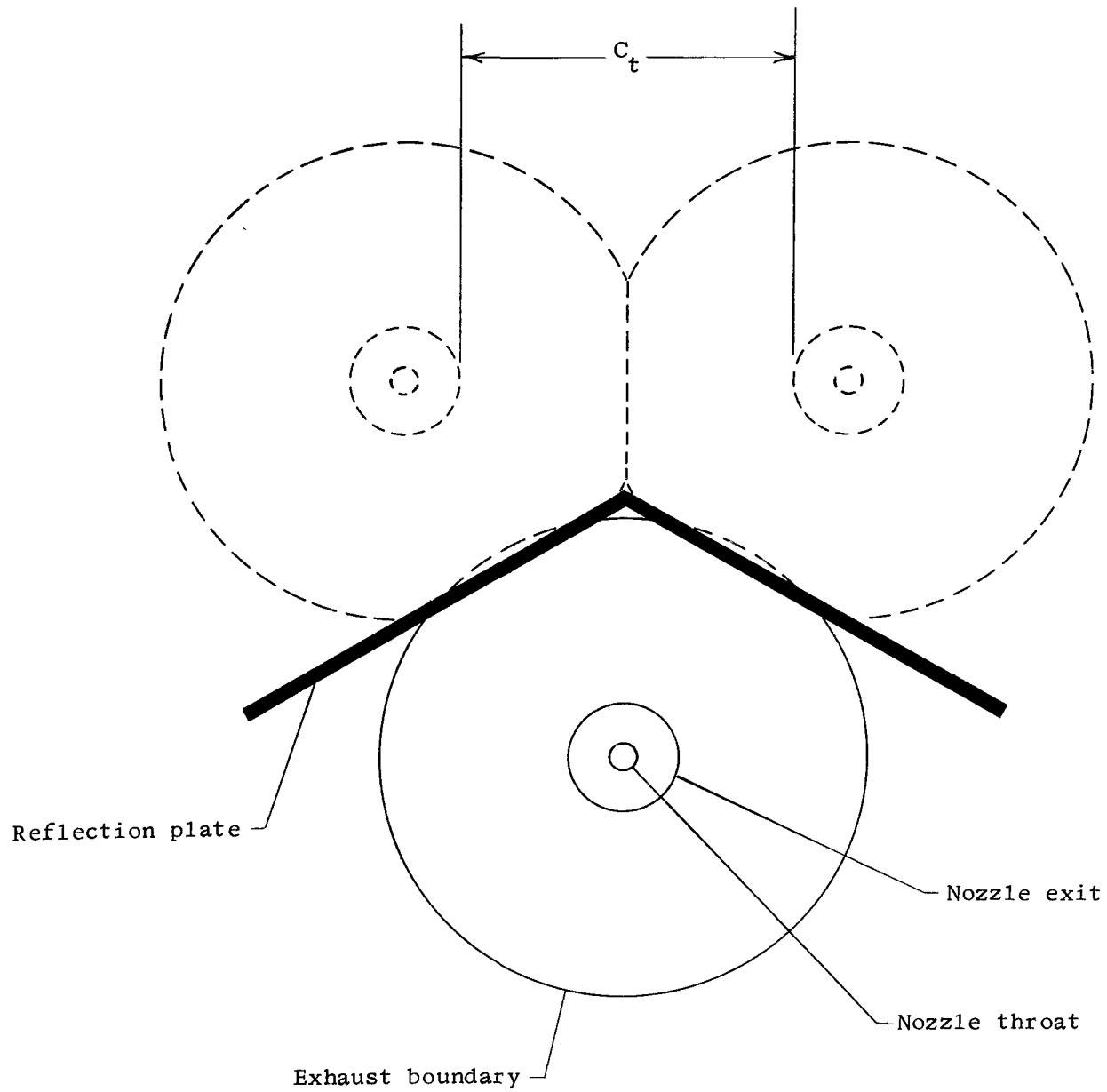

Figure 1.- Sketch showing manner in which a reflection plate was used to simulate the interference from exhaust boundaries of adjacent rocket motors. Figure not drawn to scale.

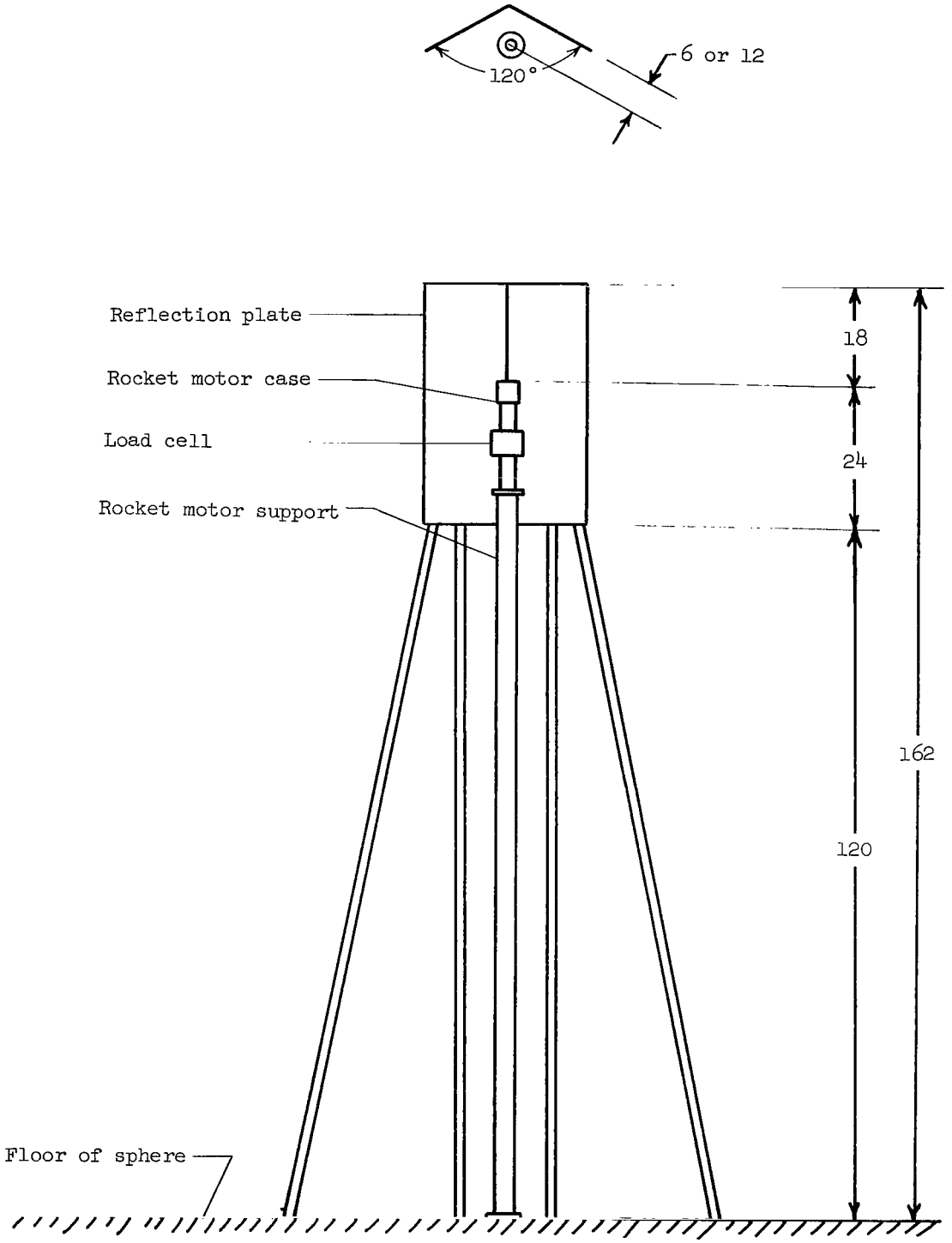

Figure 2.- Sketch of test setup. All dimensions are in inches.

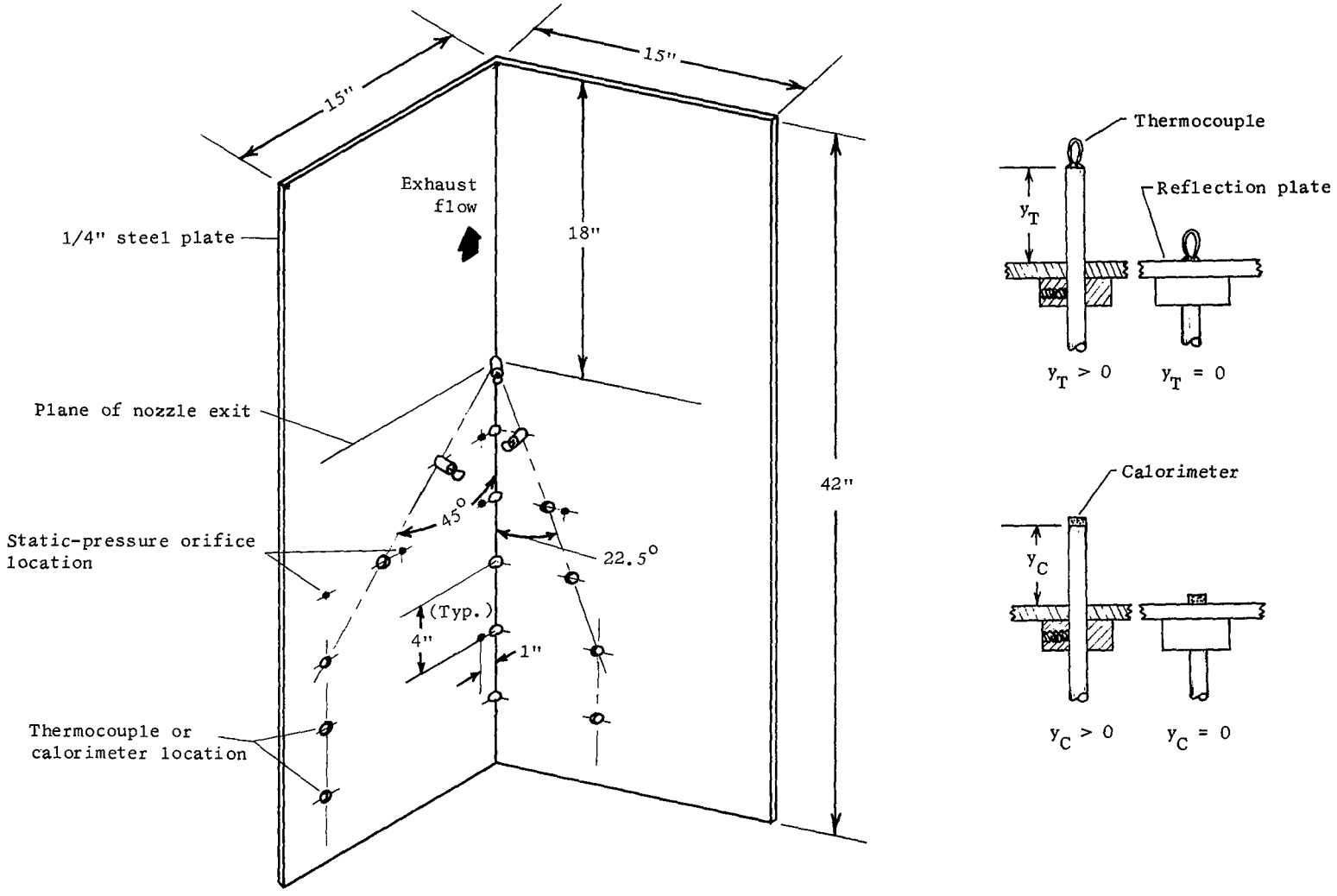

(a) Sketches showing location and typical installation of instrumentation.

Figure 3.- Reflection plate.

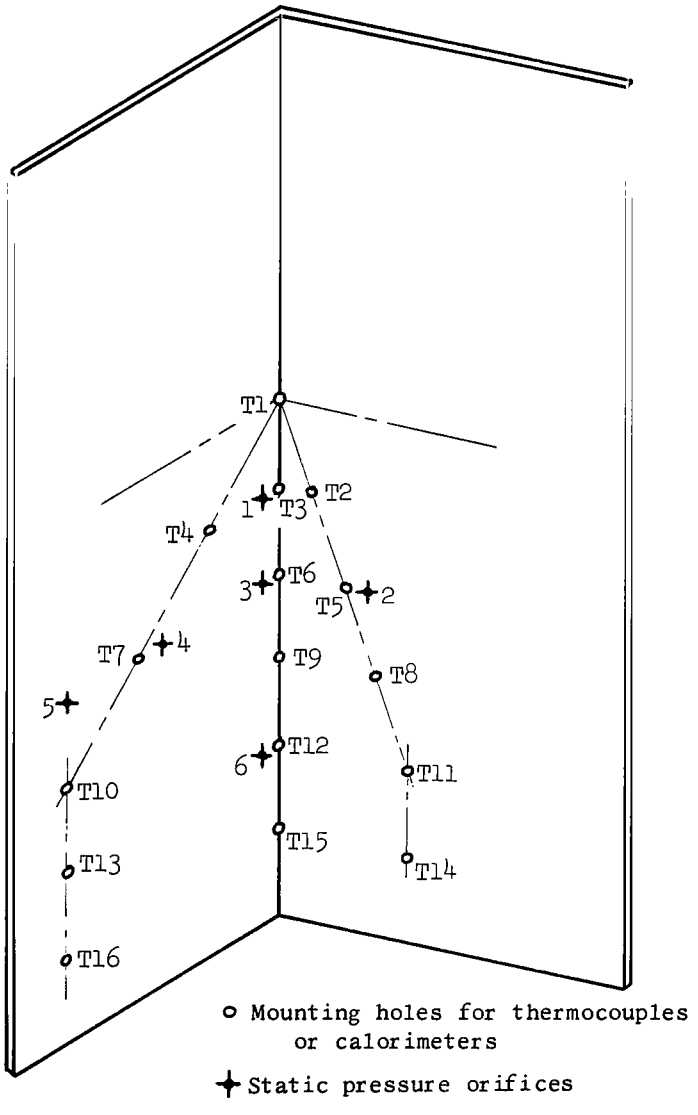

Configuration	$\frac{C_t}{d_e}$	y_T	y_C	Total-pressure probe location
I	8.02	1	1	T5
II	8.02	0	0	T6
III	8.02	0	0	T4
IV	17.05	1	1	T4
V	17.05	0	1	--

(b) Thermocouple and pressure-orifice location key.

Figure 3.- Concluded.

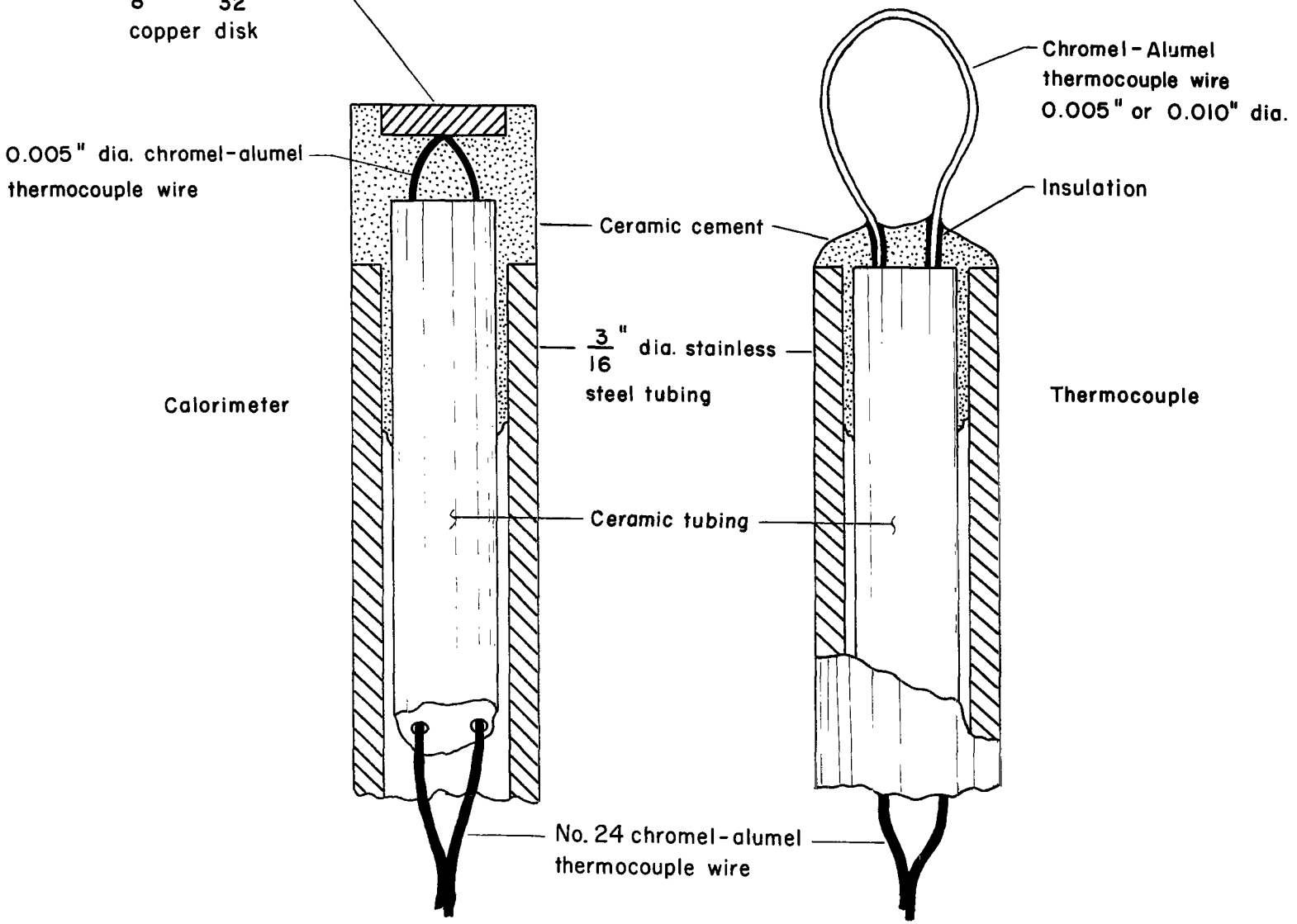

Figure 4.- Sketch showing thermocouple and calorimeter construction. Figure not drawn to scale.

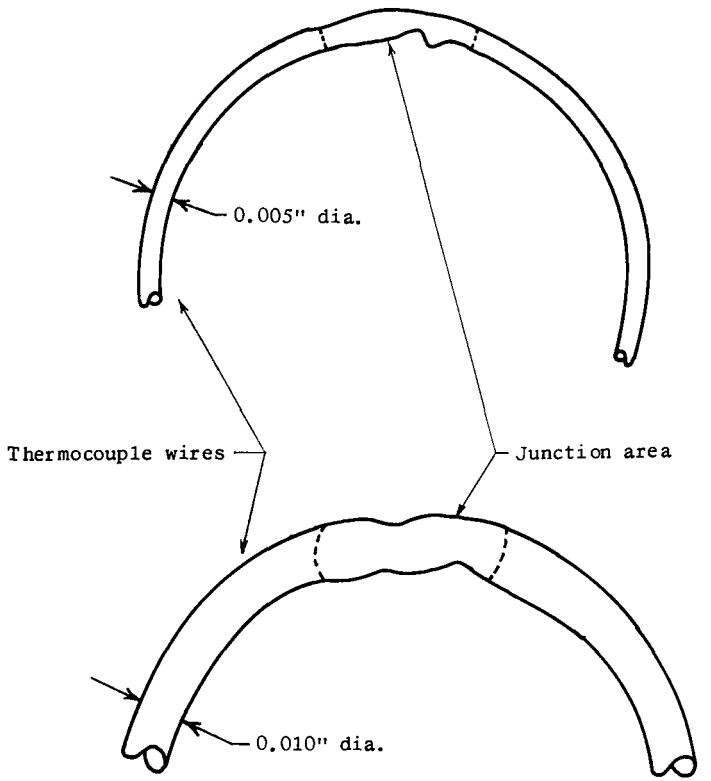

Calorimeter number	$\frac{W_c}{A}$, Btu/ft^2 °F	Configuration number				
		I	II	III	IV	V
		Location number T-				
1	0.13871	10	10	10	10	7
2	0.13729	8	8	2	2	5
3	0.13753	9	9	3	3	6
6[a]	0.13871	-	-	5	5	-

a Calorimeter mounted parallel and 1-inch above plate (disk perpendicular to backflow)

Thermocouple number	Wire diameter, in.	$\frac{d}{12}\frac{wc}{4}$, Btu/ft^2 °F	Configuration number				
			I	II	III	IV	V
			Location number T-				
1	0.010	0.01224	1	1	1	1	1
2			2	2	8	8	2
3			3	3	9	9	3
4			4	4	6	6	4
5			6	5	-	-	14
6			7	7	7	7	15
7			11	11	11	11	16
11	0.005	0.00612	15	15	15	15	11
12			13	13	13	13	9
13			16	16	16	16	13
14			12	12	12	12	8
16			14	14	14	14	10
18			← Sphere →				

Figure 5.- Enlarged silhouettes of typical thermocouple junction areas and tables of thermocouple and calorimeter properties and locations.

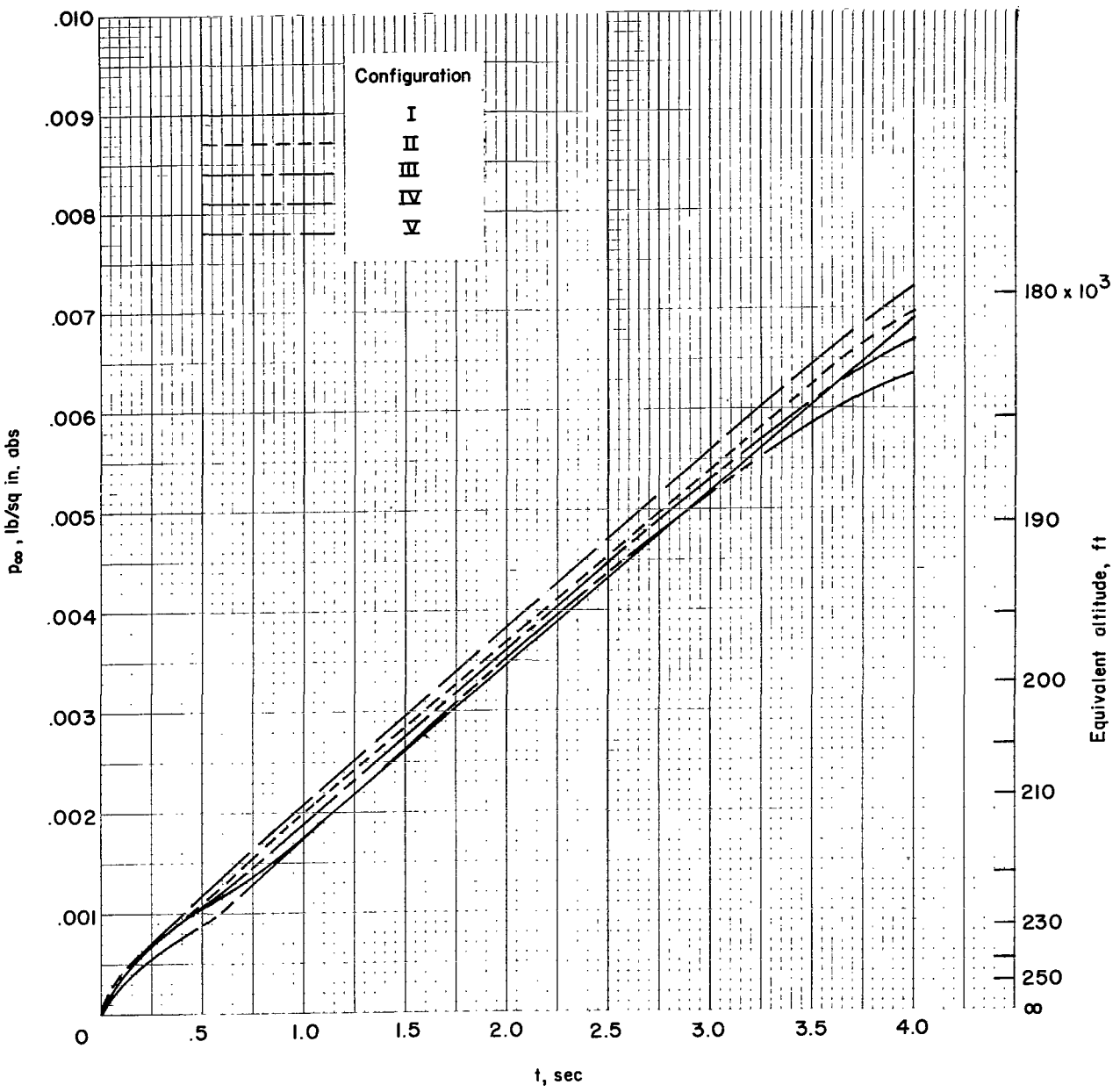

Figure 6.- Variation of sphere pressure with time.

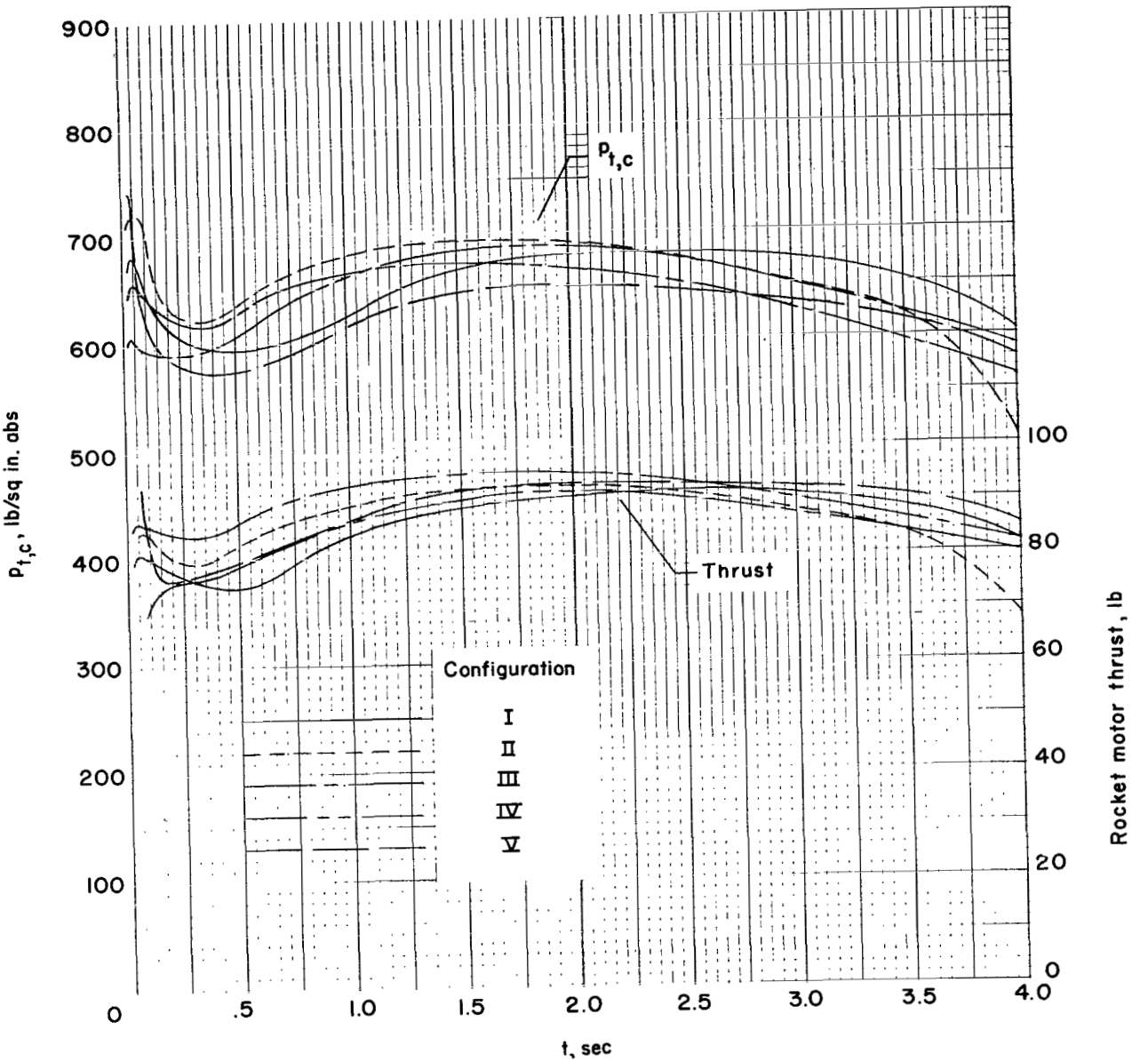

Figure 7.- Variation of rocket combustion chamber pressure and thrust with time.

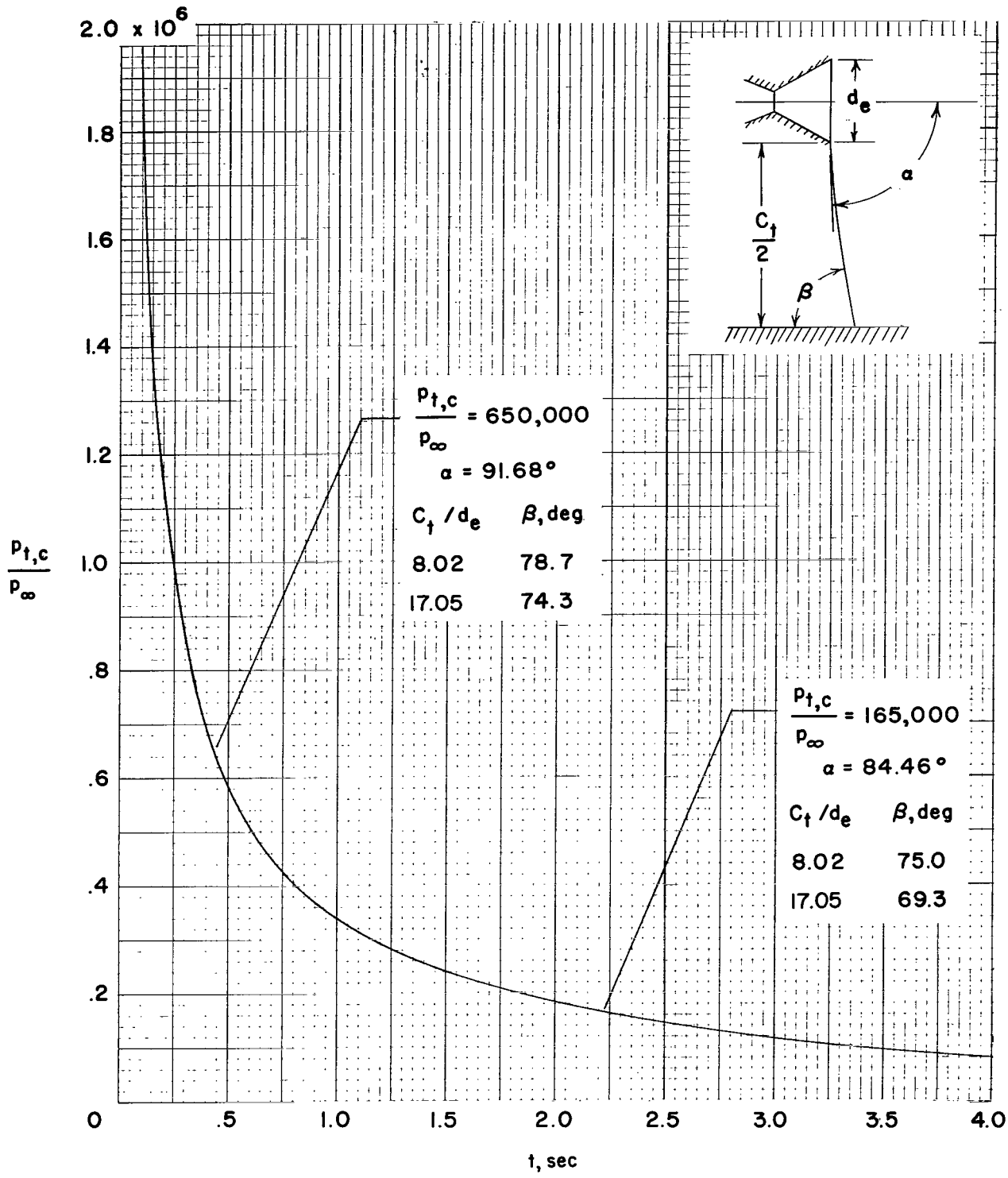

Figure 8.- Nozzle pressure ratio variation with time for median values of sphere pressure and rocket-motor combustion chamber pressure.

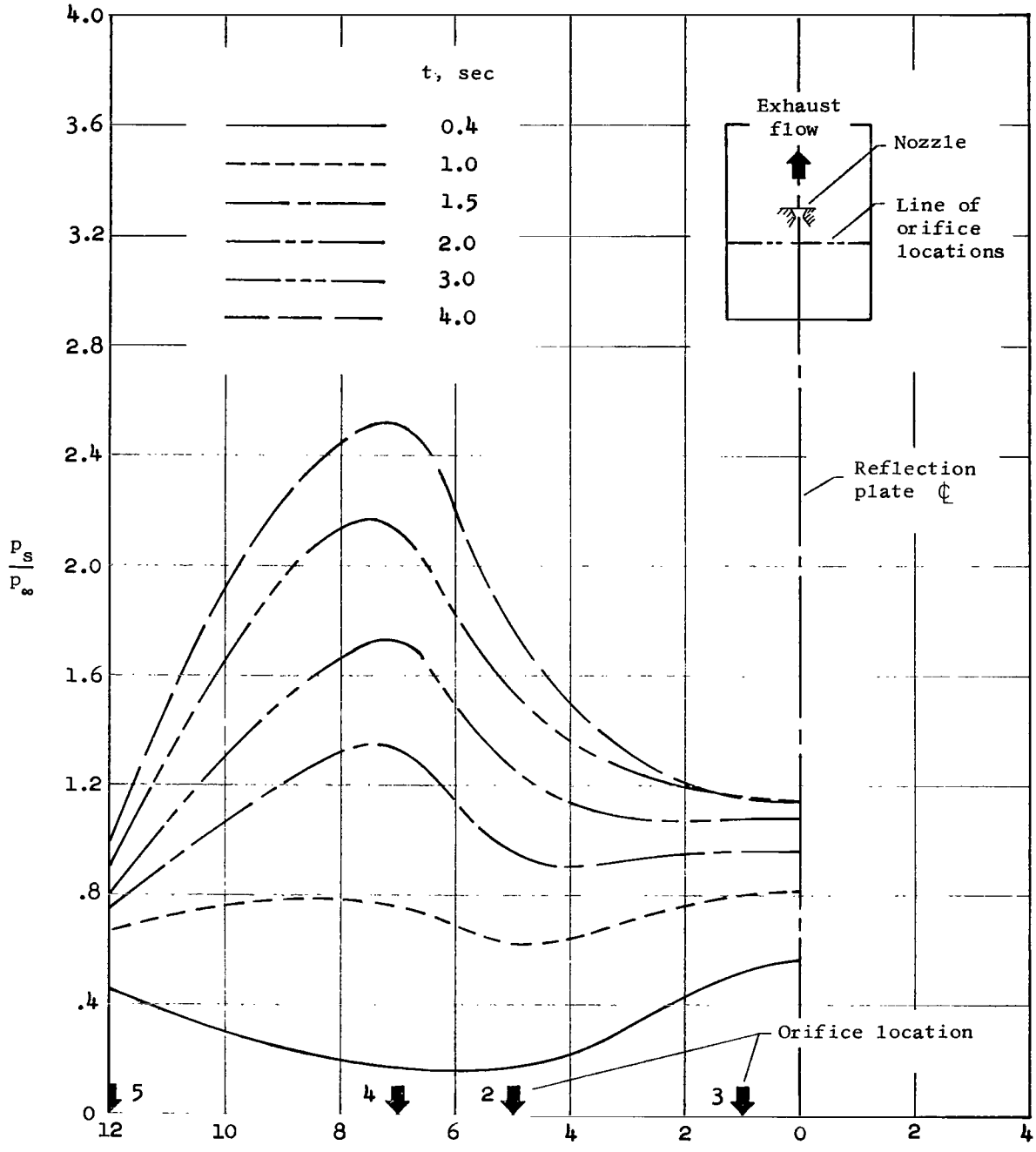

(a) $\frac{C_t}{d_e} = 8.02$.

Figure 9.- Pressure distributions across reflection plate 8 inches upstream from nozzle exit.

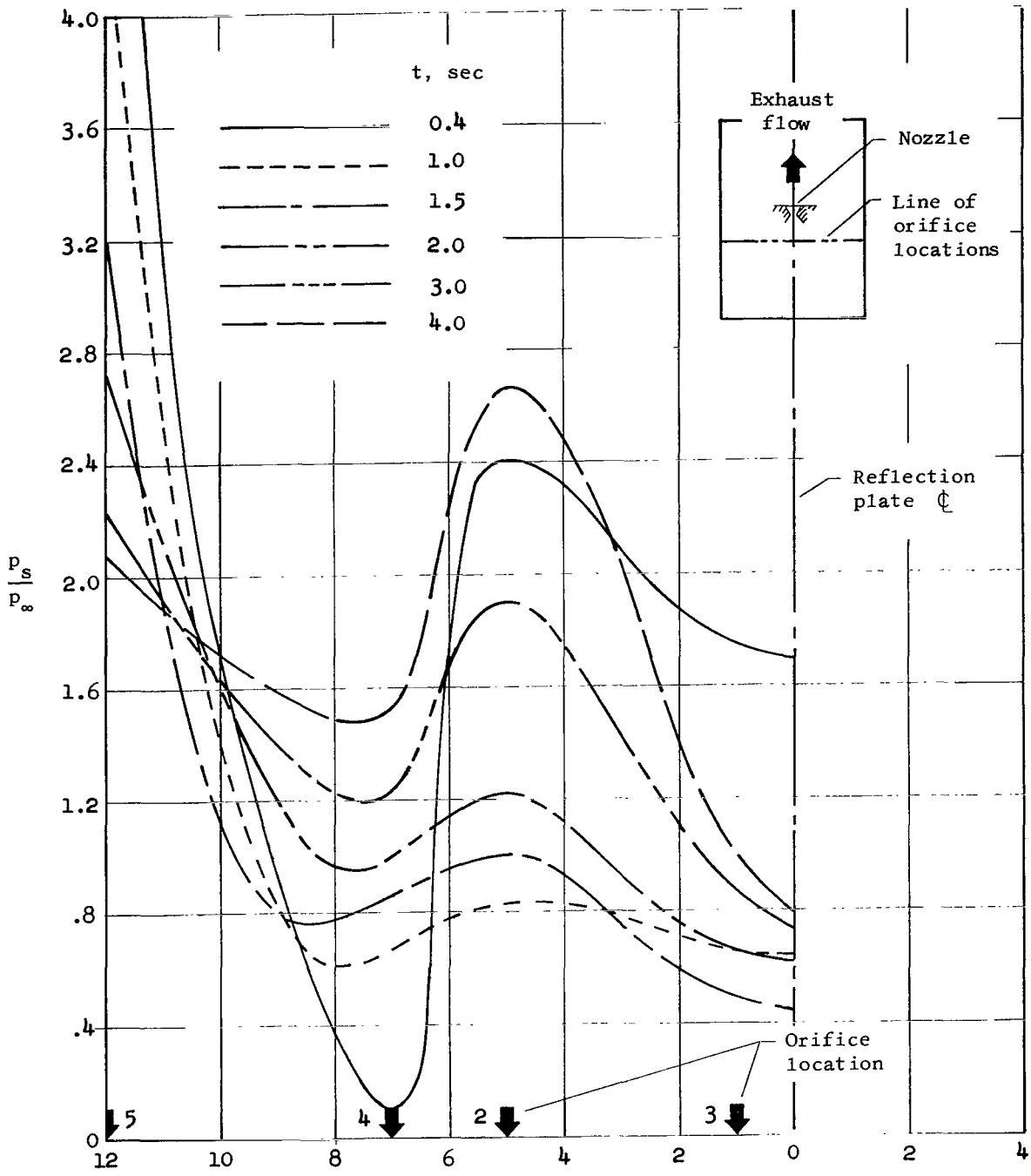

(b) $\frac{Ct}{d_e} = 17.05$.

Figure 9.- Concluded.

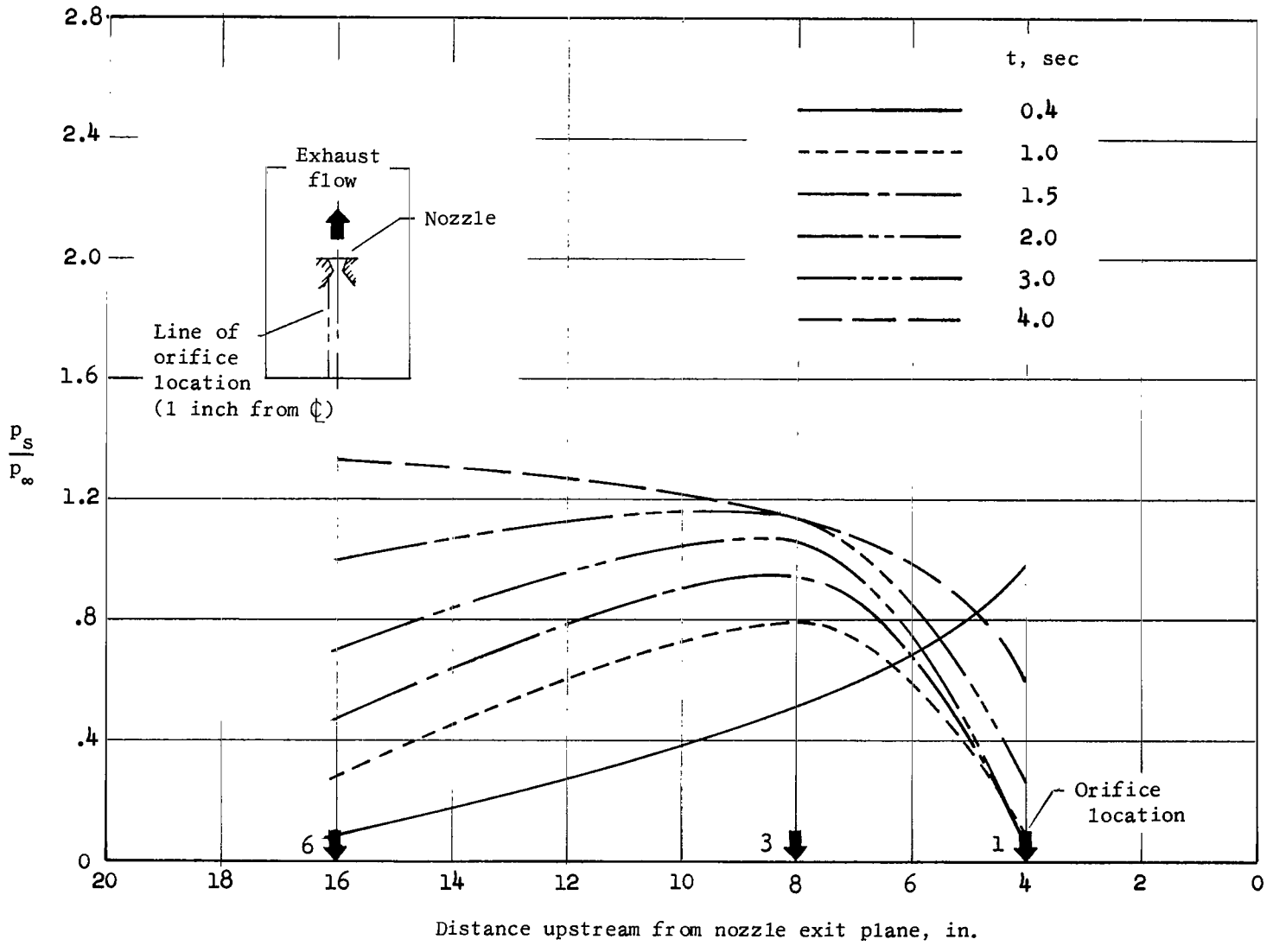

(a) $\frac{C_t}{d_e} = 8.02$.

Figure 10.- Pressure distributions parallel to reflection plate center line.

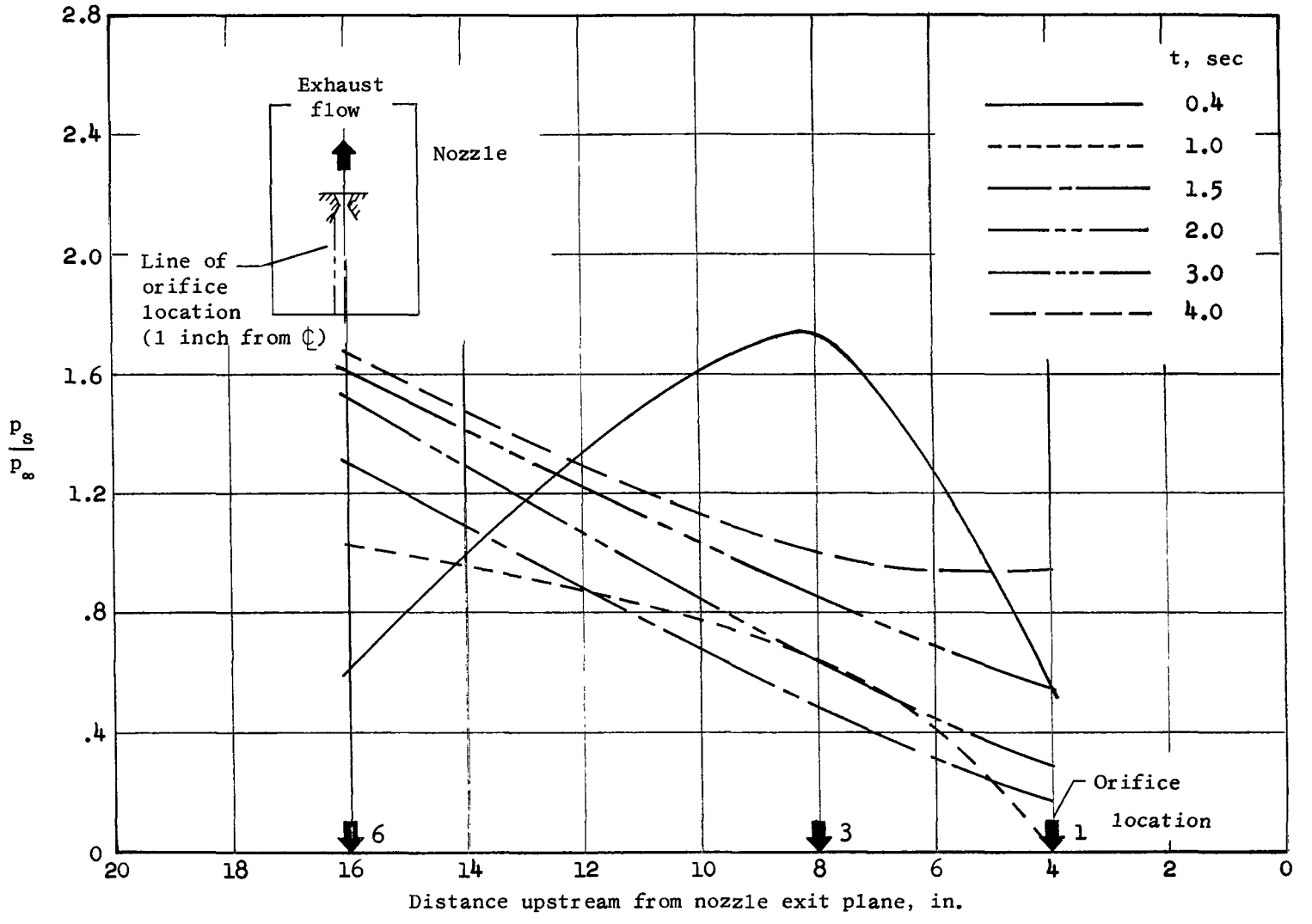

(b) $\frac{C_t}{d_e} = 17.05$.

Figure 10.- Concluded.

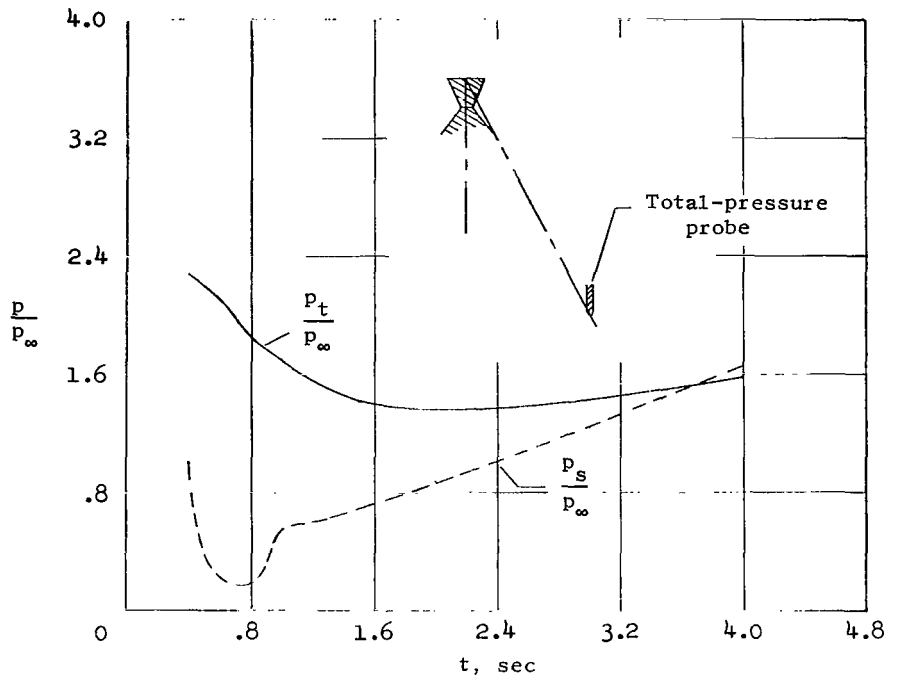

(a) Configuration I.

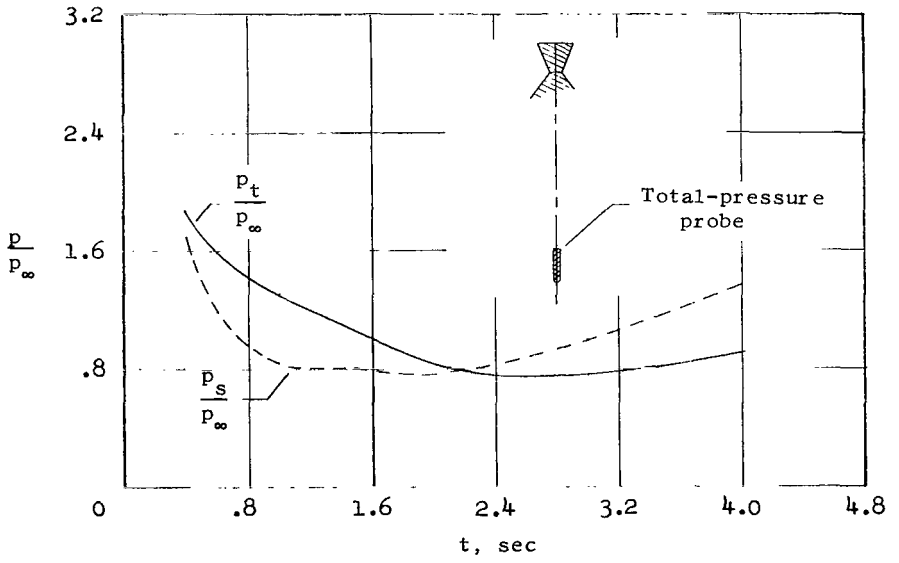

(b) Configuration II.

Figure 11.- Total and static pressures in exhaust backflow.

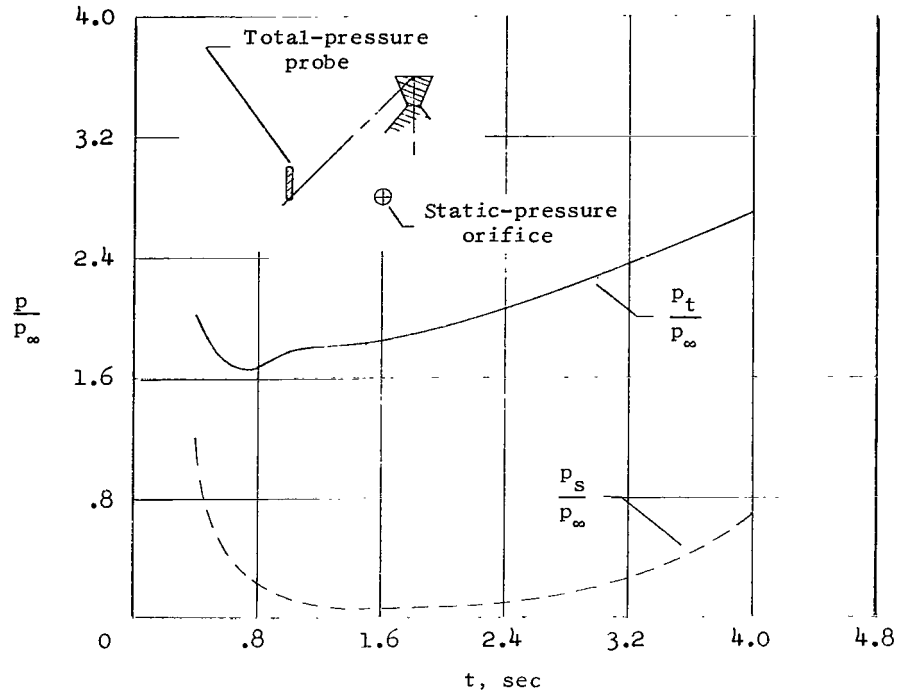

(c) Configuration III.

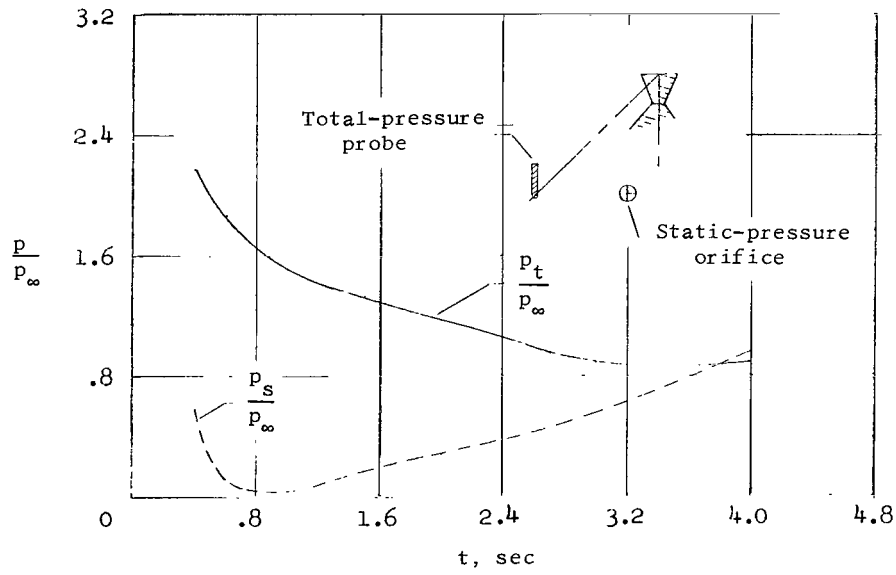

(d) Configuration IV.

Figure 11.- Concluded.

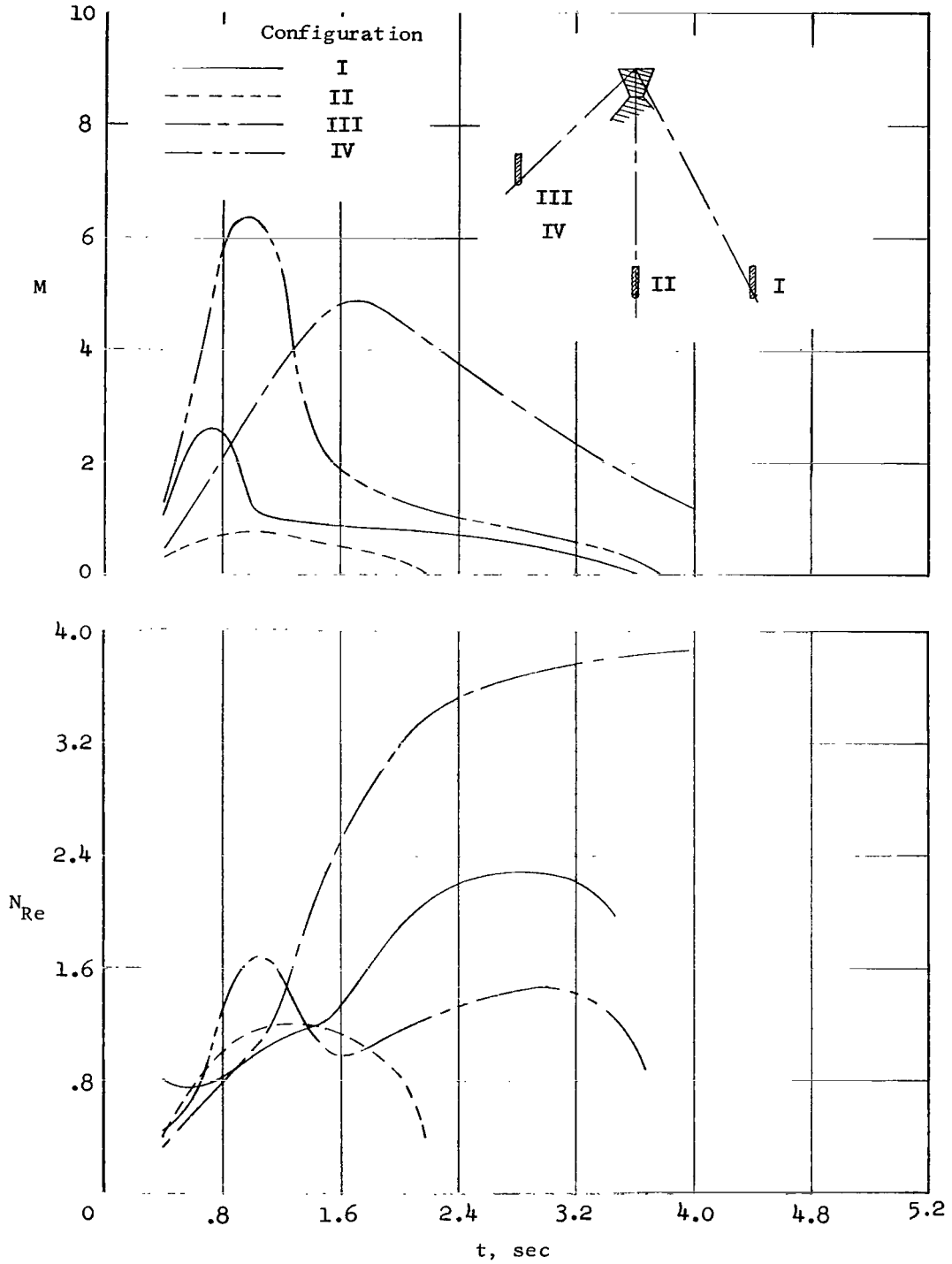

Figure 12.- Backflow Mach number and unit Reynolds number variation with time. Mach number curves for configurations III and IV obtained from static-pressure assumption. See figures 11(c) and 11(d) and text.

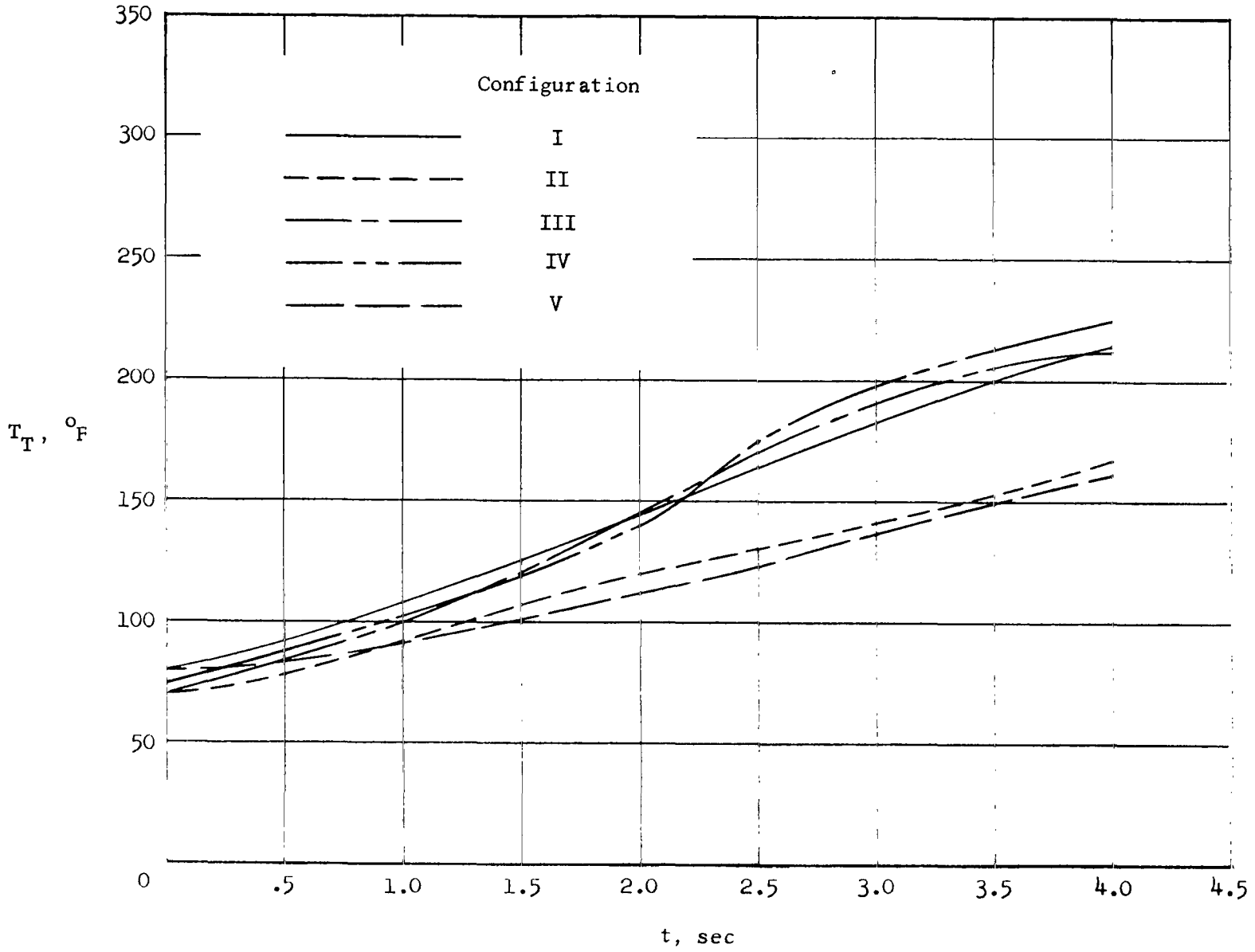

Figure 13.- Sphere thermocouple temperature time histroy d_T = 0.005 in.

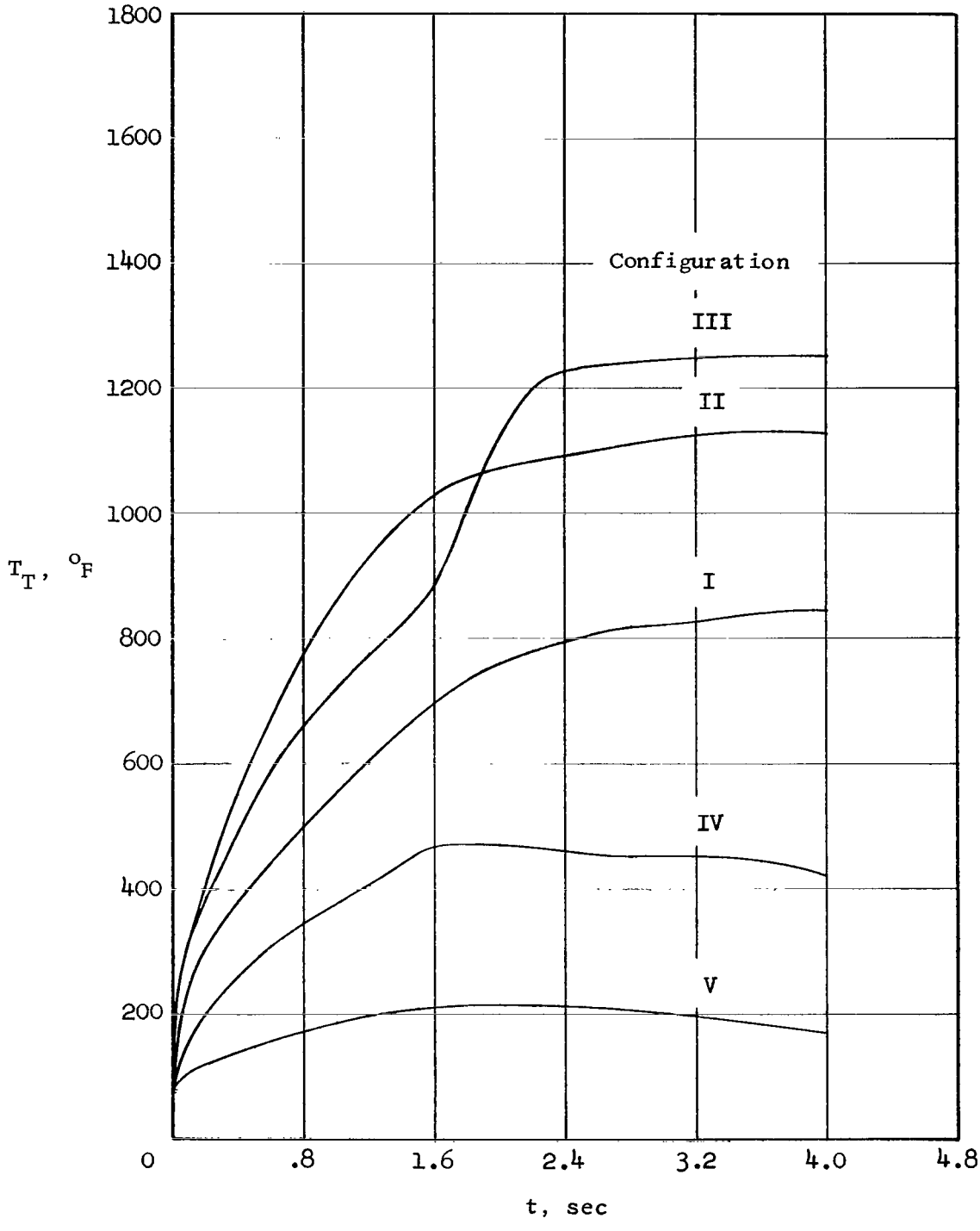

Figure 14.- Position T1 thermocouple temperature time history d_T = 0.010 in.

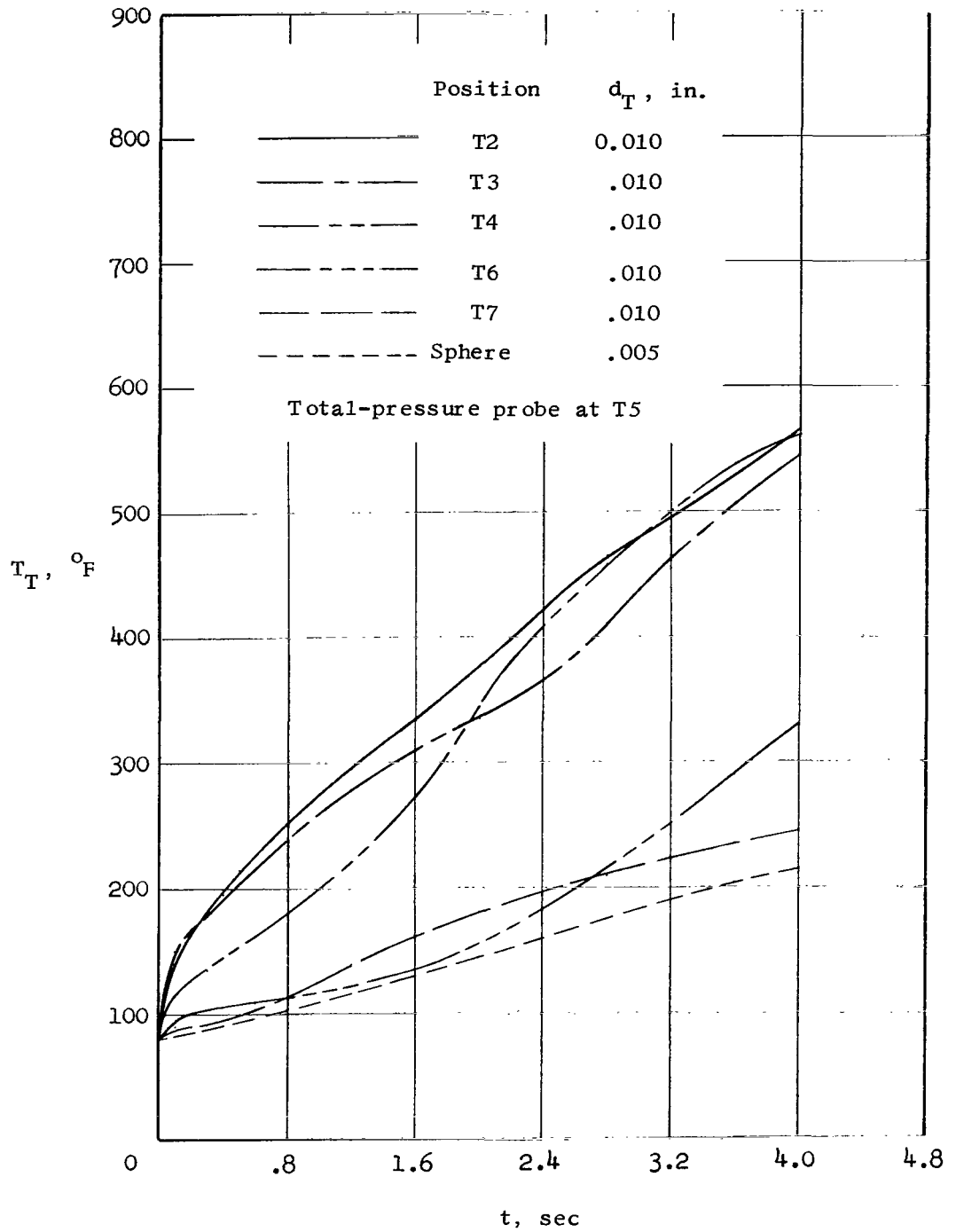

(a) Positions T2 to T4, T6, and T7.

Figure 15.- Thermocouple and heat-meter temperature time histories. Configuration I.

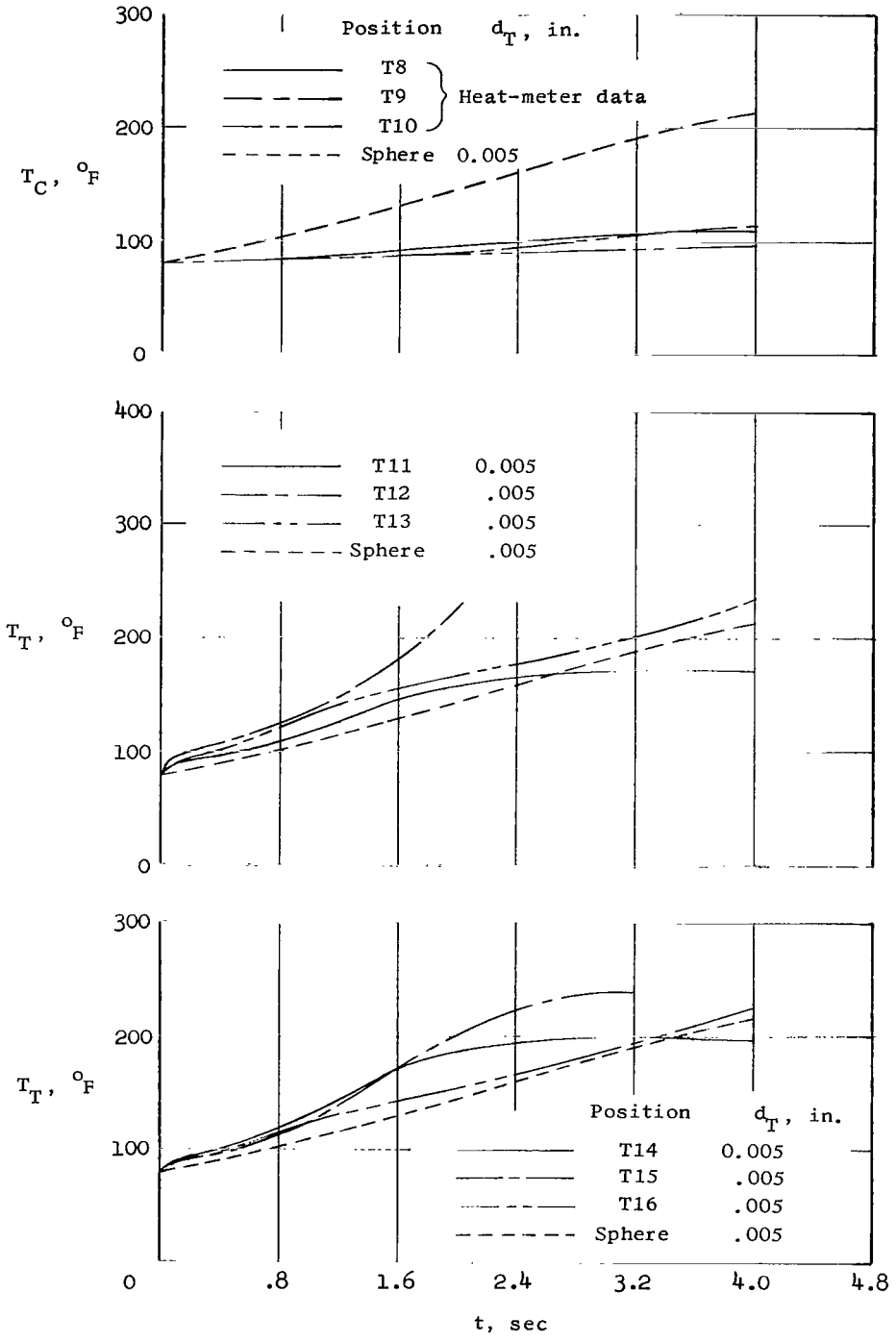

(b) Positions T8 to T16.

Figure 15.- Concluded.

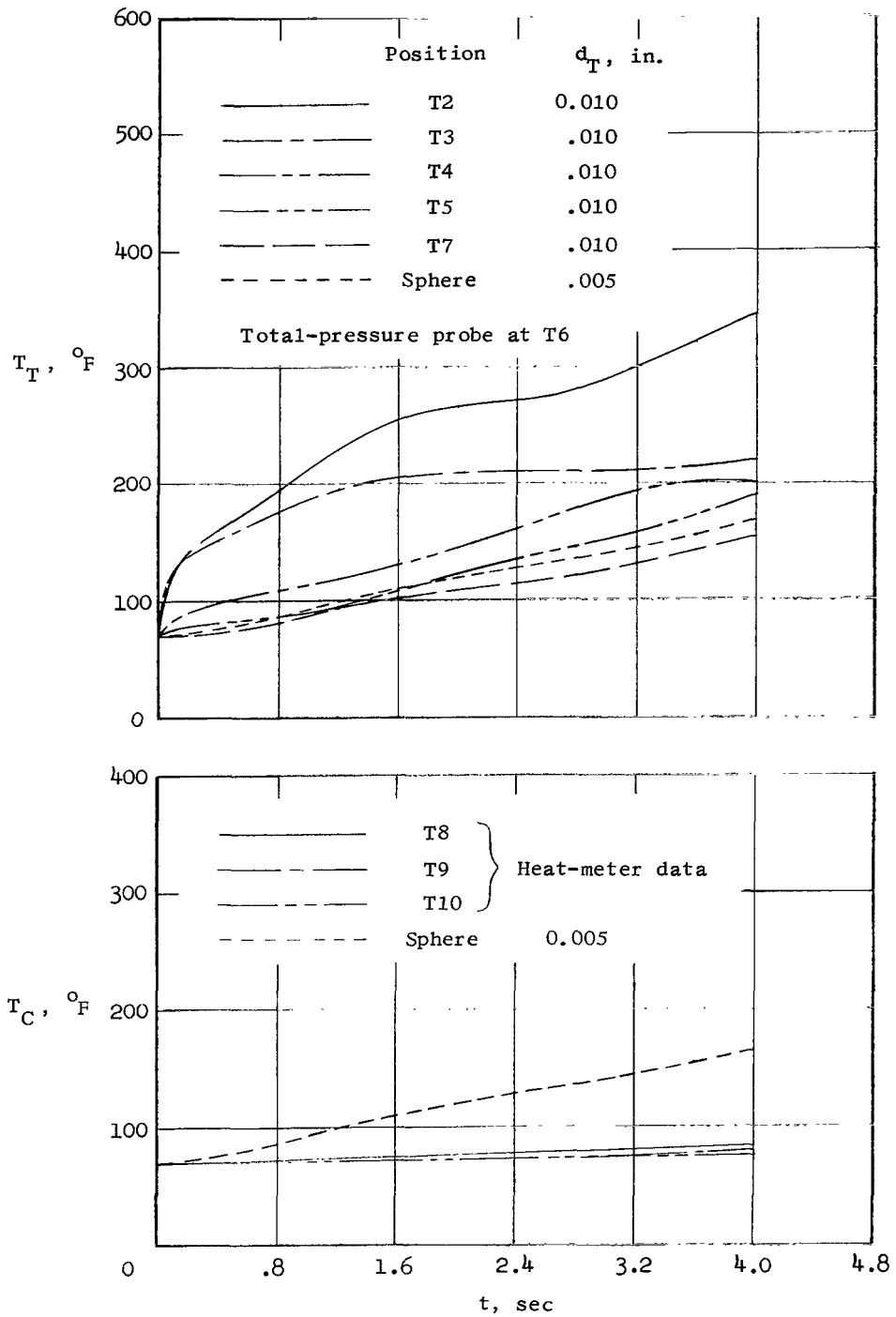

(a) Positions T2 to T10.

Figure 16.- Thermocouple and heat-meter temperature time histories. Configuration II.

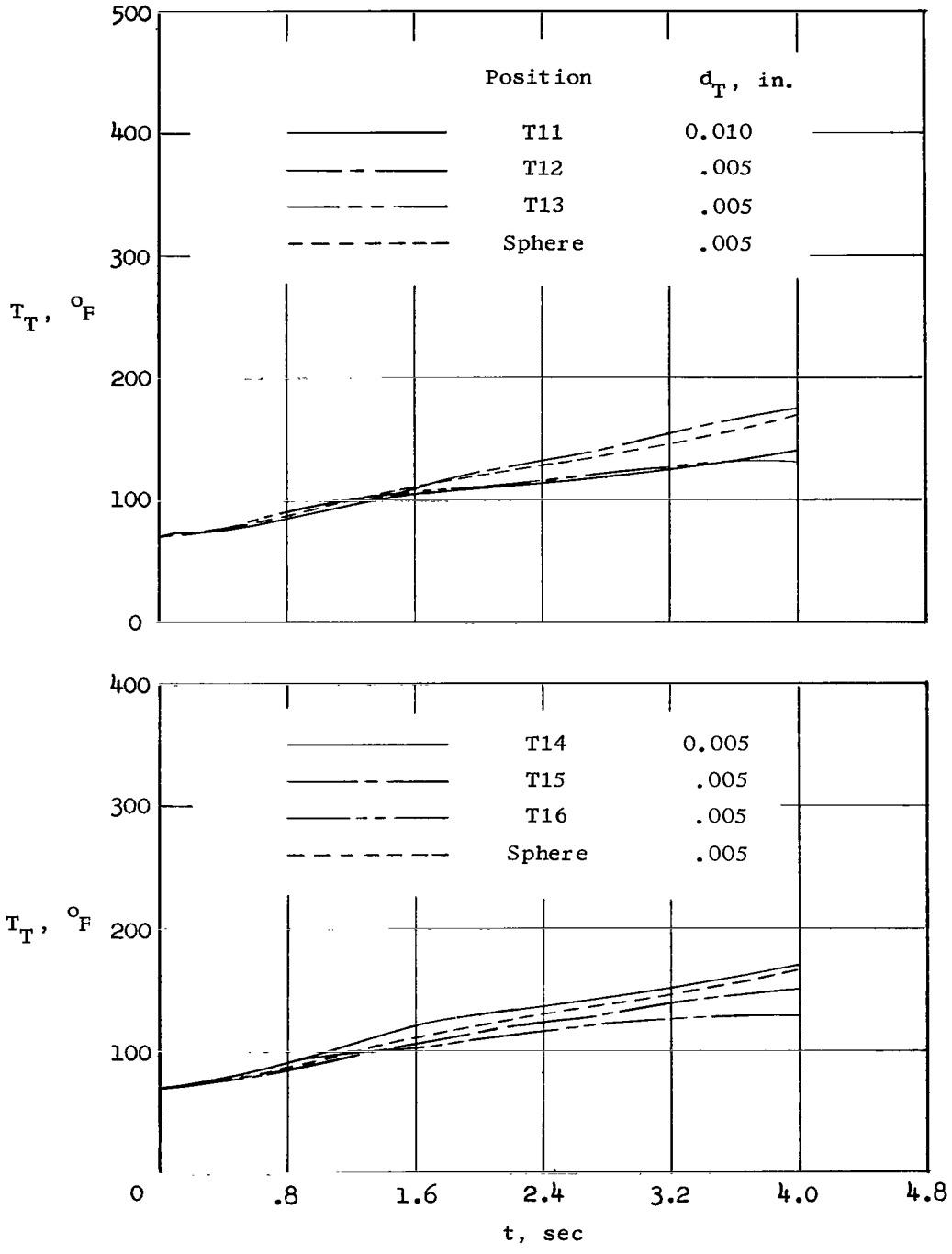

(b) Positions T11 to T16.

Figure 16.- Concluded.

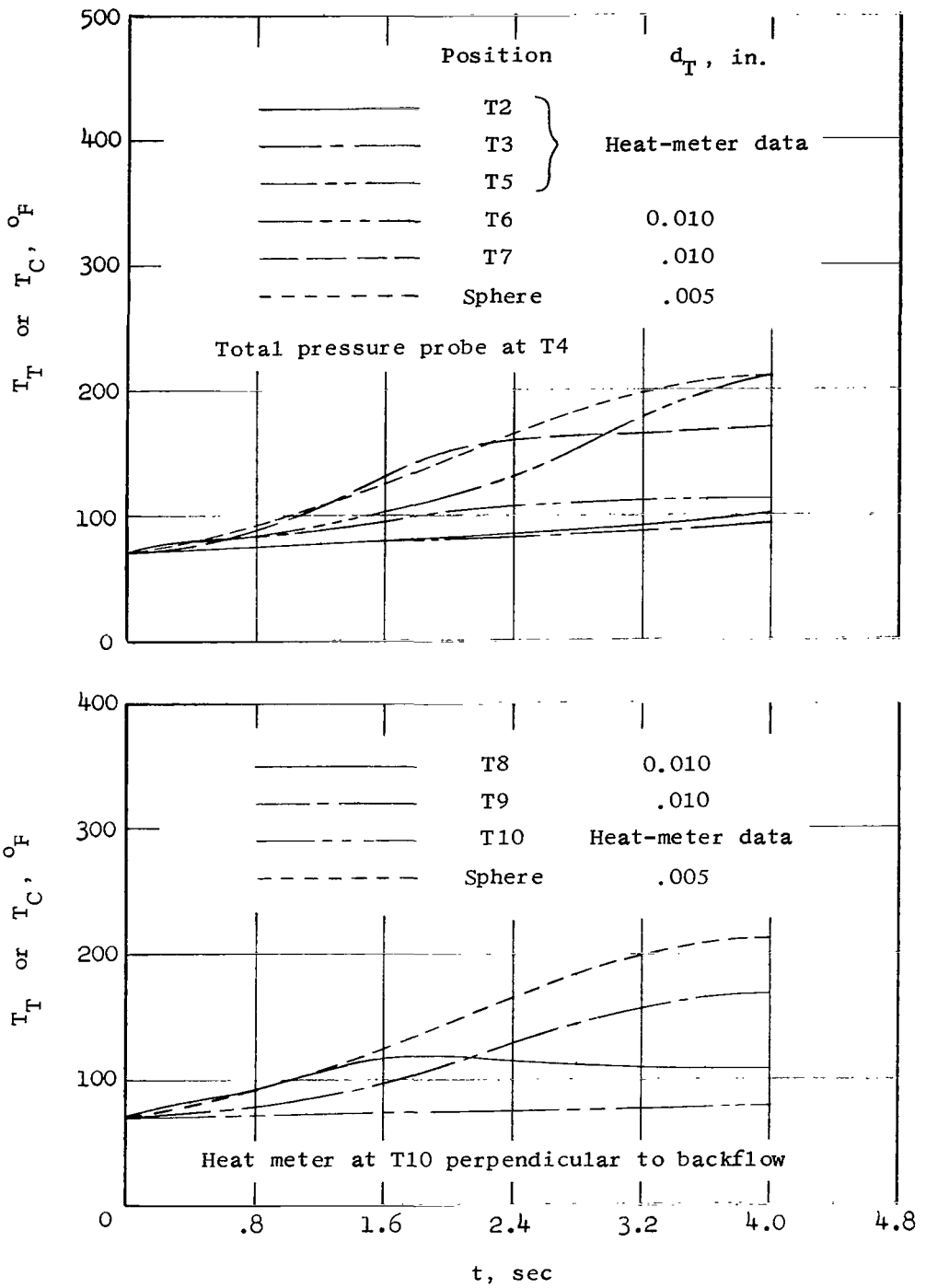

(a) Positions T2 to T10.

Figure 17.- Thermocouple and heat-meter temperature time histories. Configuration III.

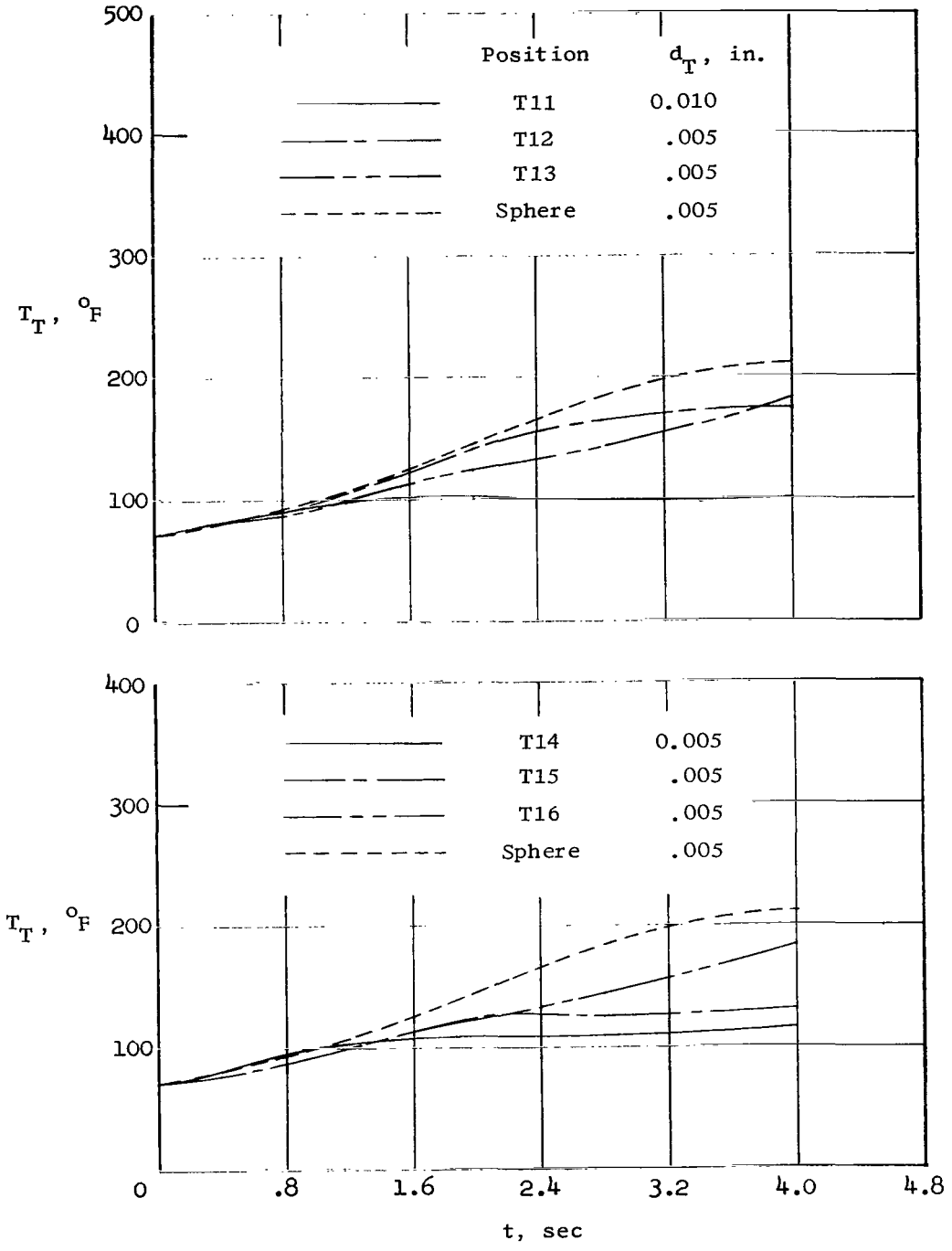

(b) Positions T11 to T16.

Figure 17.- Concluded.

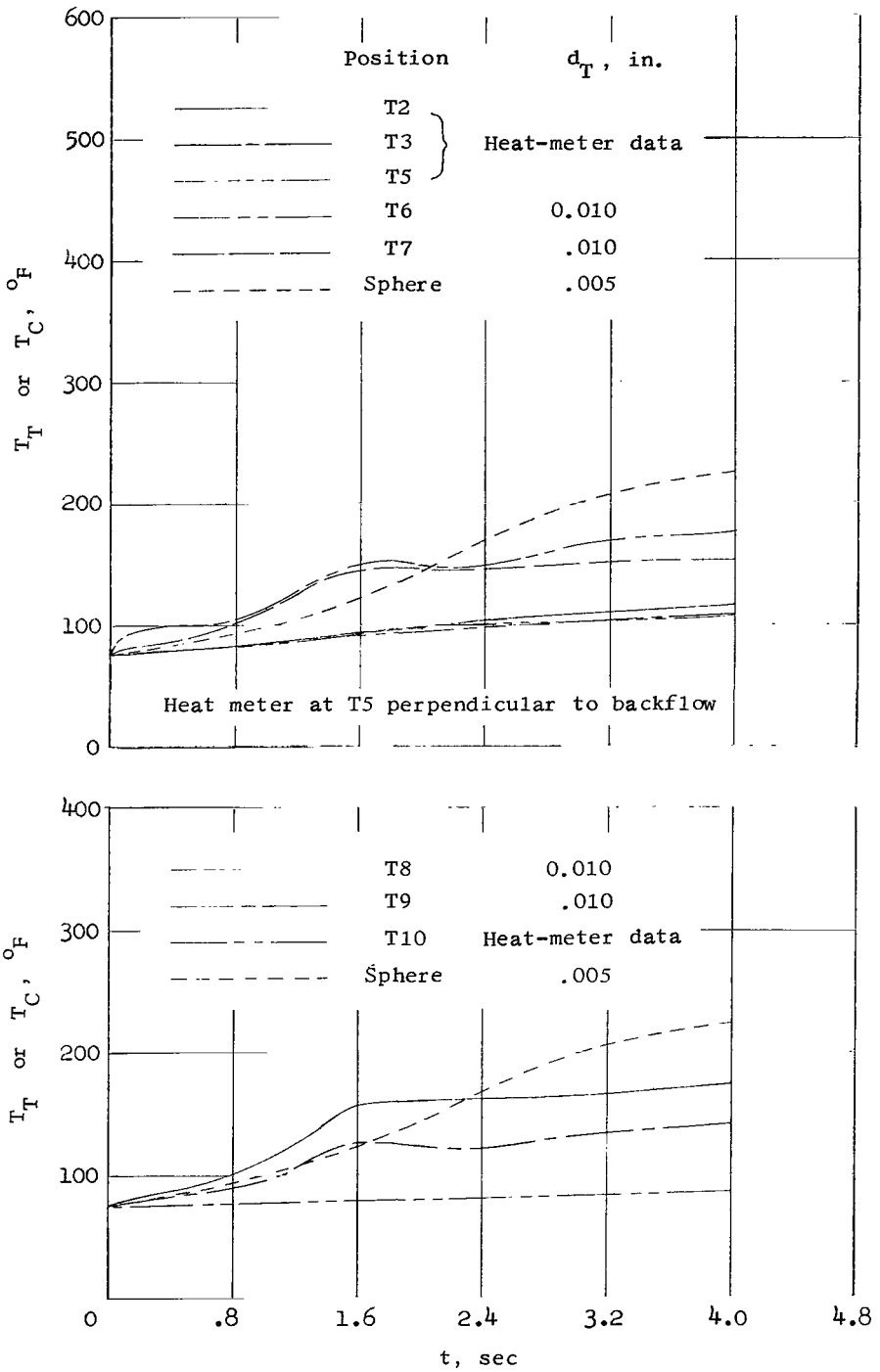

(a) Positions T2 to T10.

Figure 18.- Thermocouple and heat-meter temperature time histories. Configuration IV.

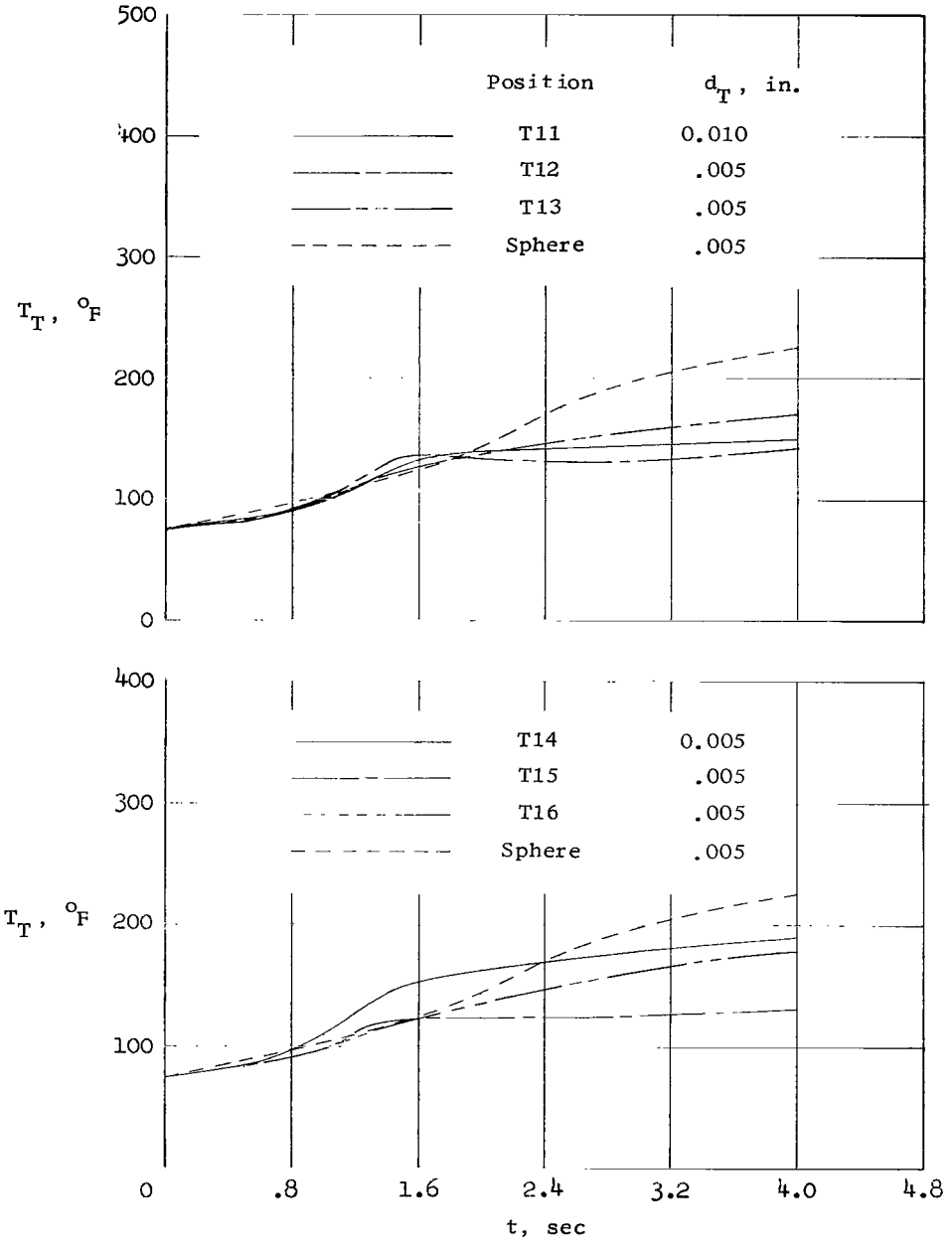

(b) Positions T11 to T16.

Figure 18.- Concluded.

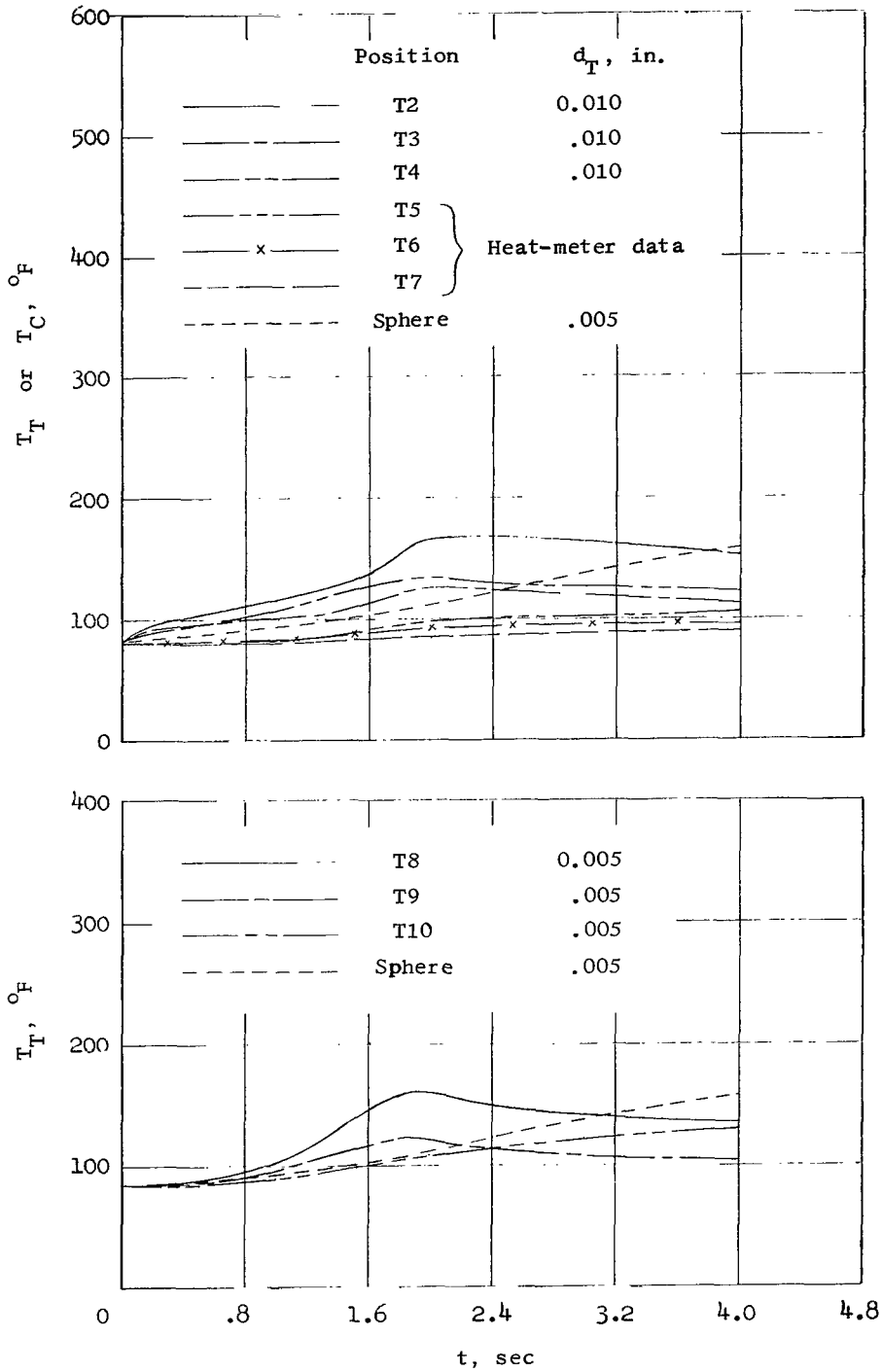

(a) Positions T2 to T10.

Figure 19.- Thermocouple and heat-meter temperature time histories. Configuration V.

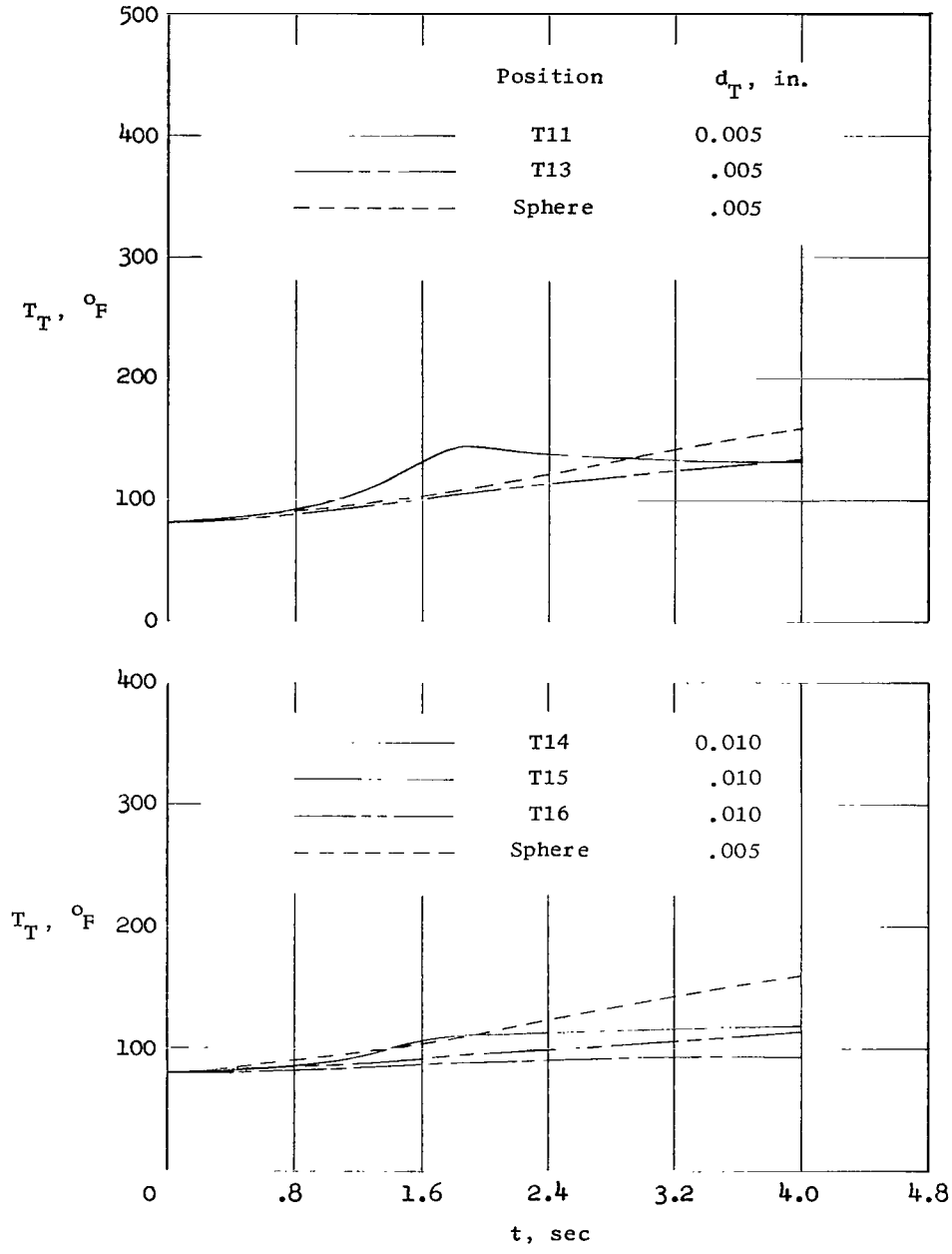

(b) Positions T11 to T16.

Figure 19.- Concluded.

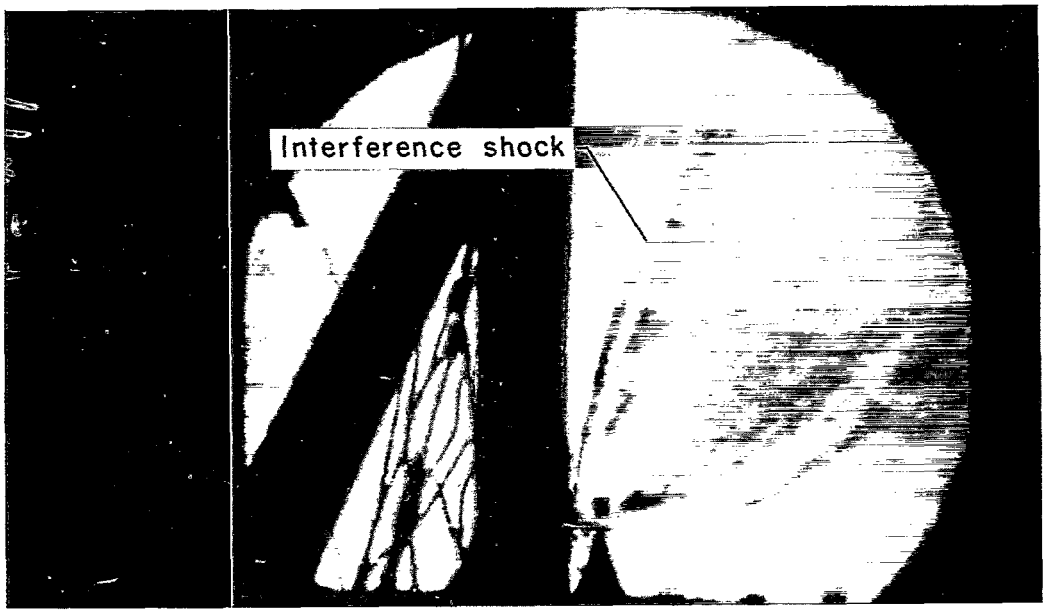

Single sonic nozzle, $p_e/p_\infty \approx 5 \times 10^4$

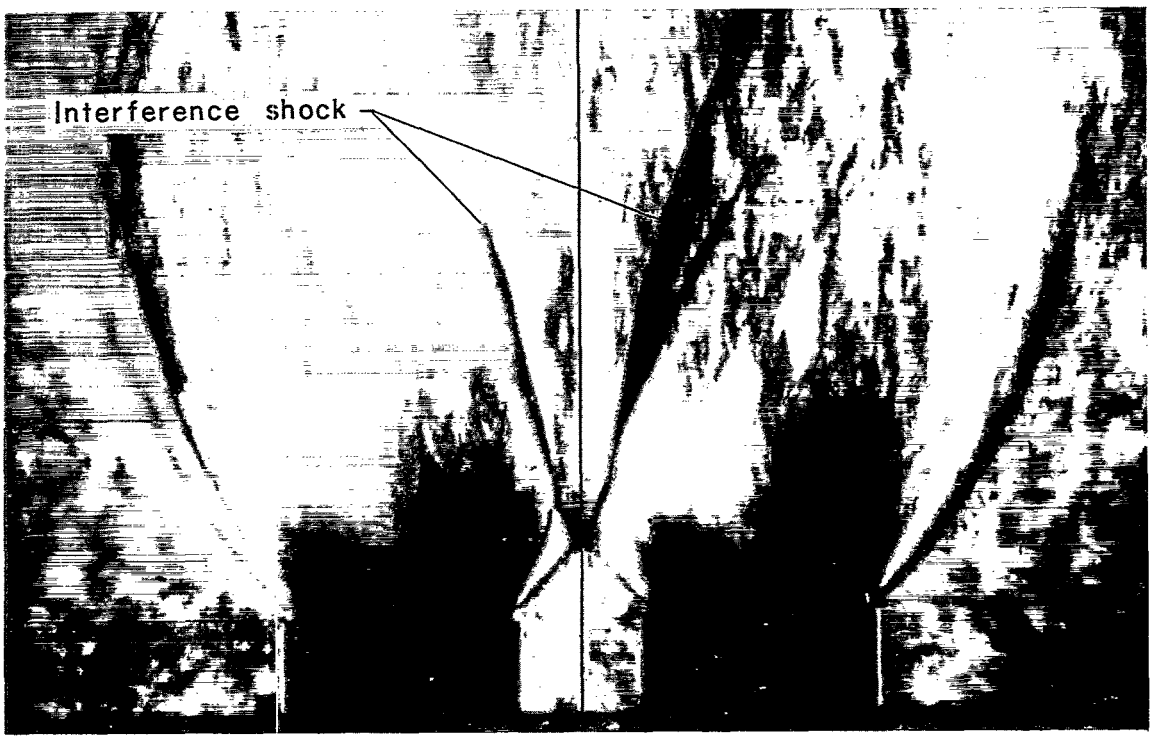

Cluster of 4 sonic nozzles, $p_e/p_\infty \approx 20$

L-65-145

Figure 20.- Similarity between interference shocks with and without reflection plate.

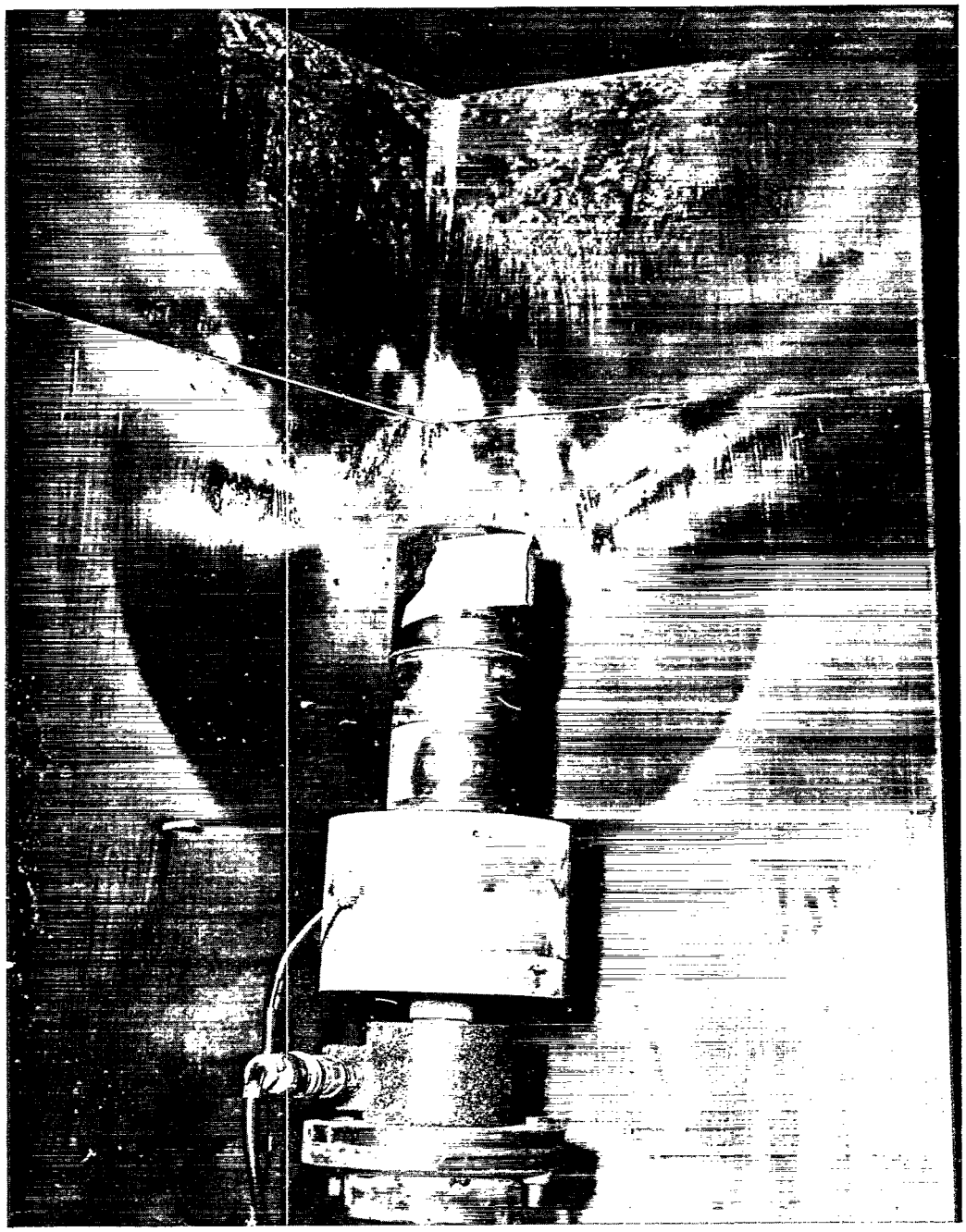

(a) Photograph of dust pattern on reflection plate. $\frac{C_t}{d_e} = 8.02$. L-62-4383

Figure 21.- Flow model.

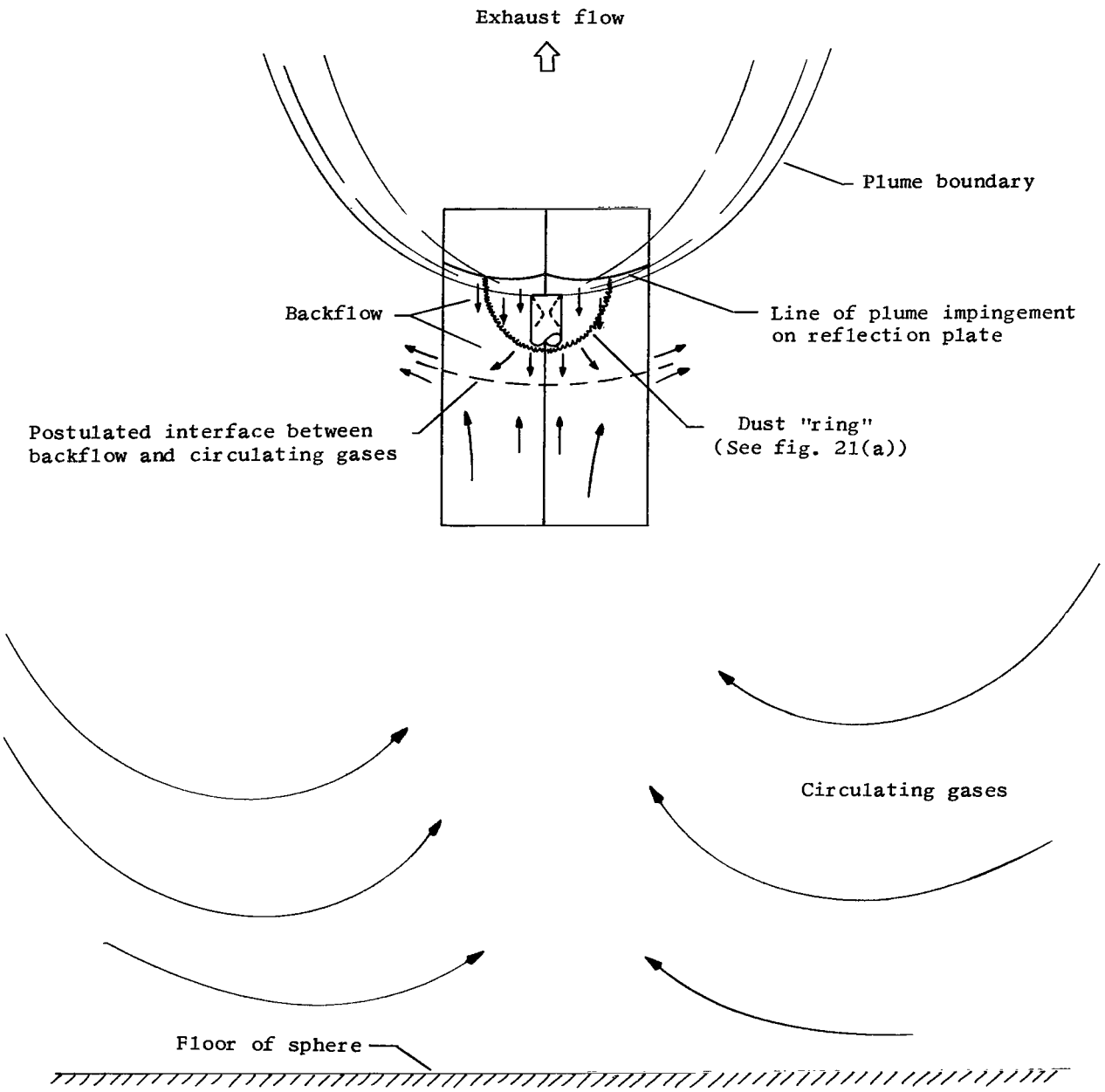

(b) Sketch for flow model discussion.

Figure 21.- Concluded.

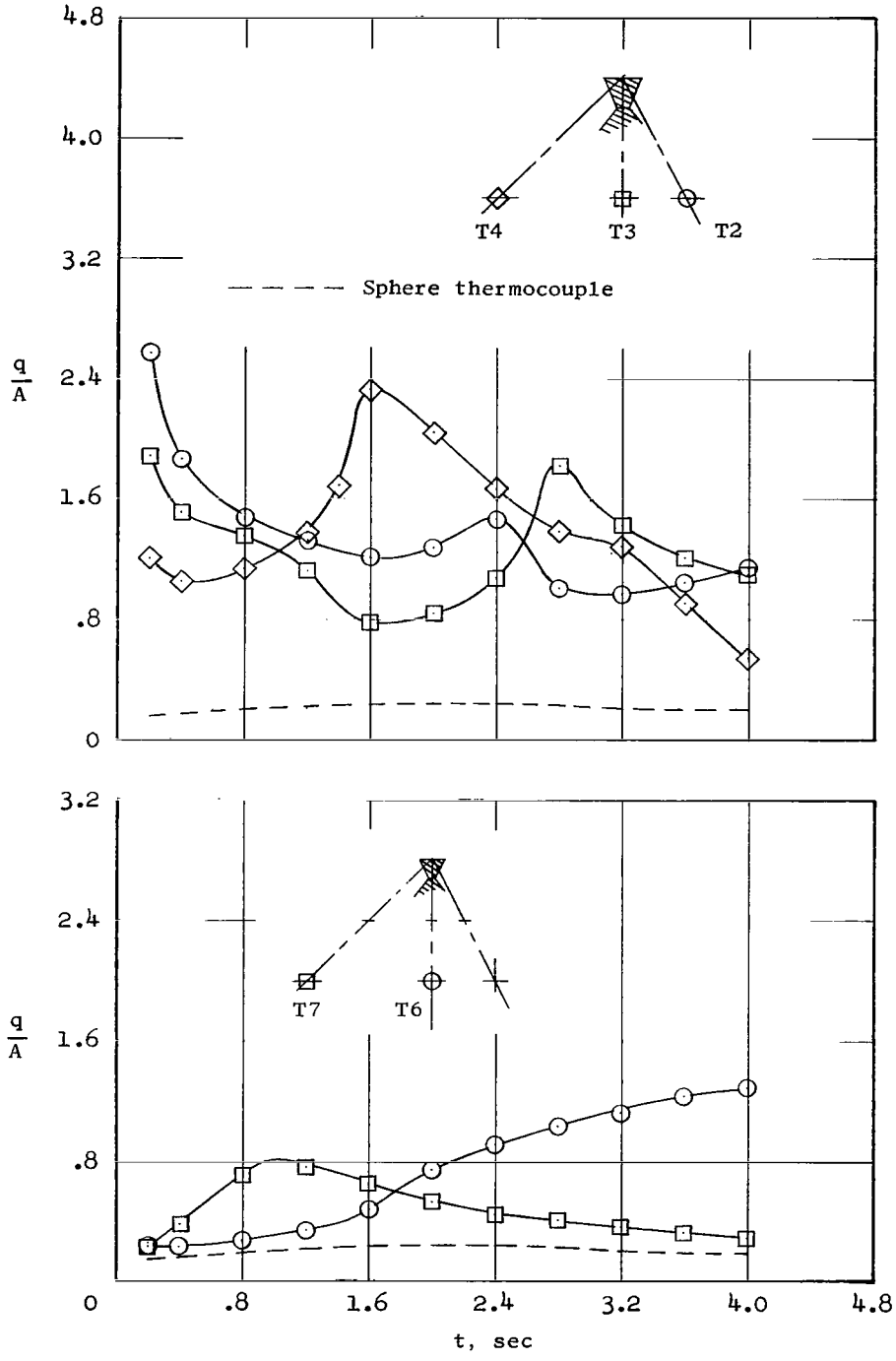

(a) Positions T2 to T4, T6, and T7.

Figure 22.- Heat flux variation with time. Configuration I.

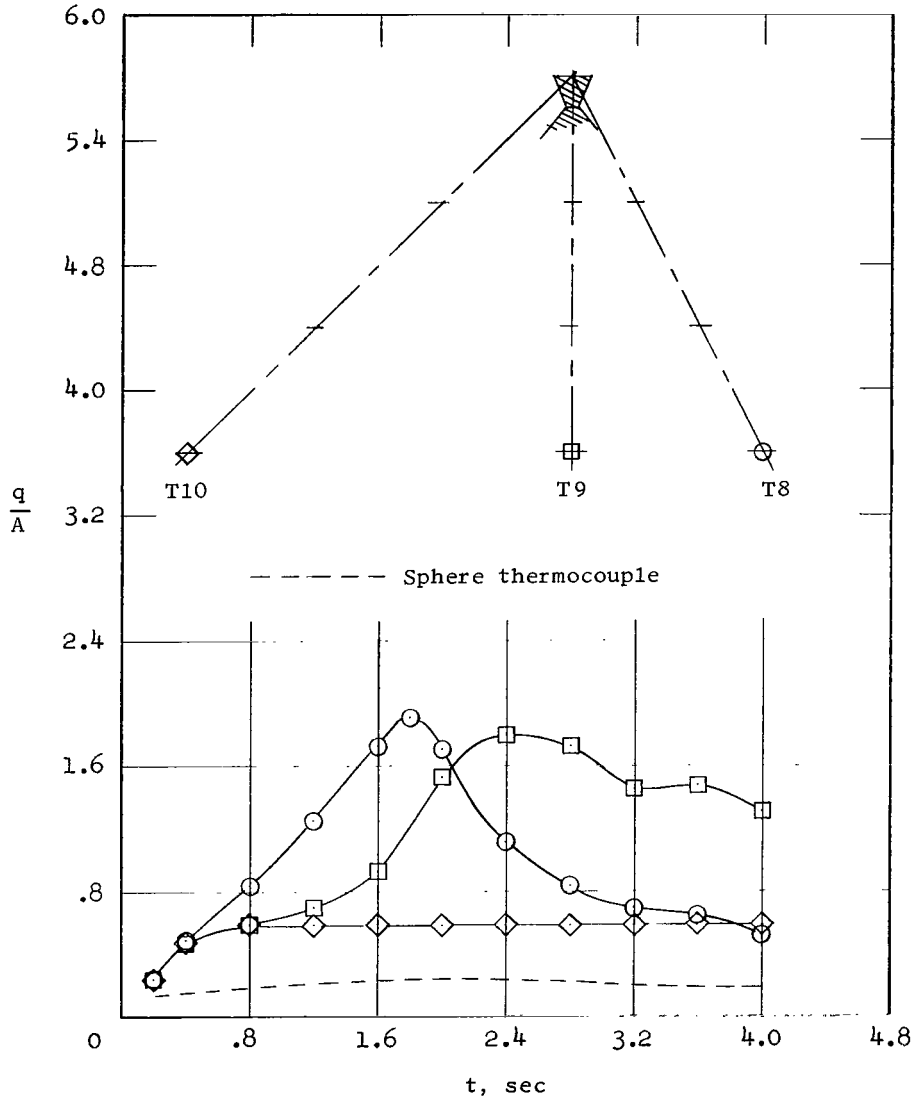

(b) Positions T8, T9, and T10.

Figure 22.- Continued.

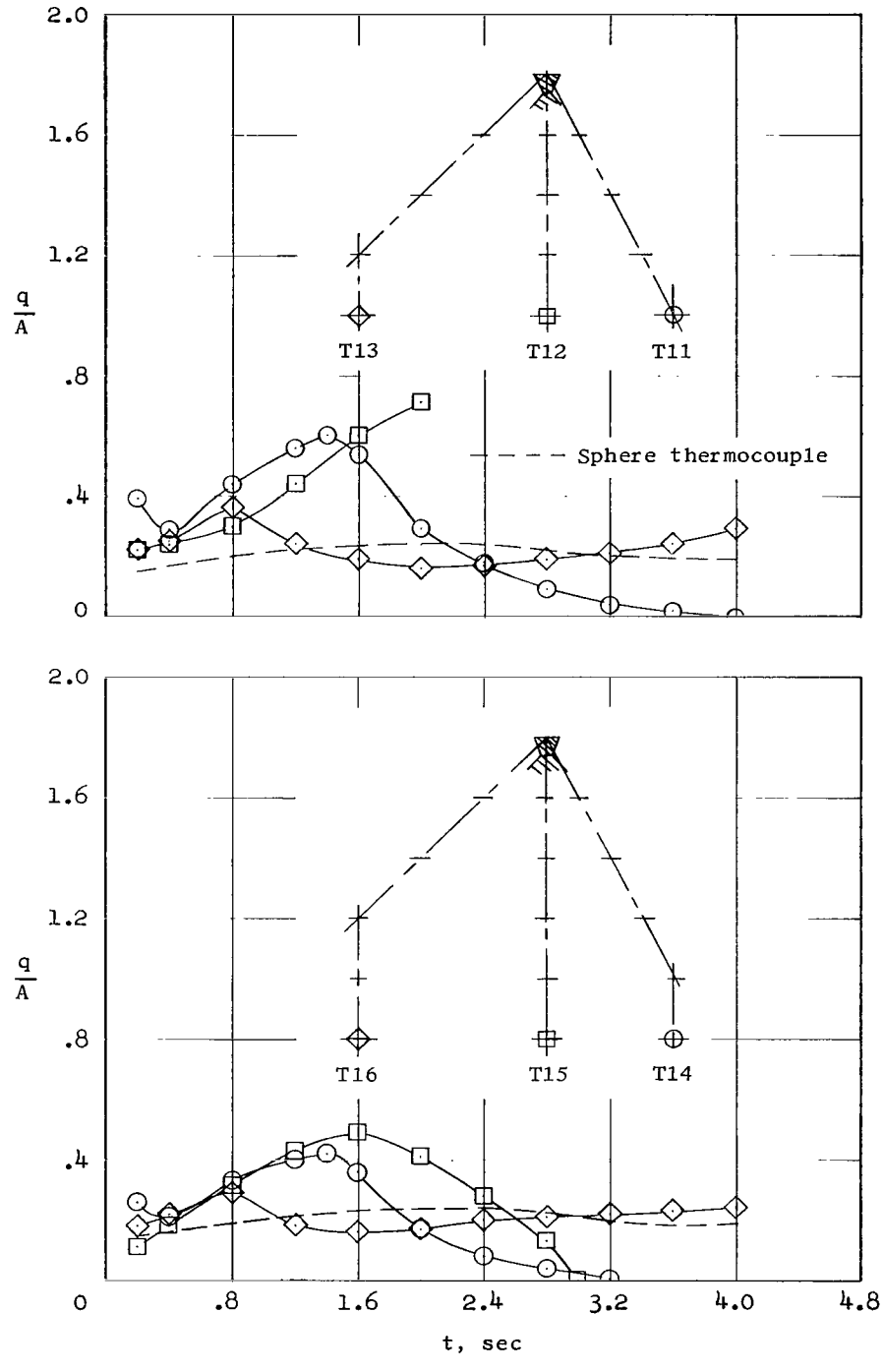

(c) Positions T11 to T16.

Figure 22.- Concluded.

Calorimeter data

Position	h, Btu/ft^2-sec-$^\circ$F
T8	1.67×10^{-4}
T9	1.27×10^{-4}
T10	1.25×10^{-4}

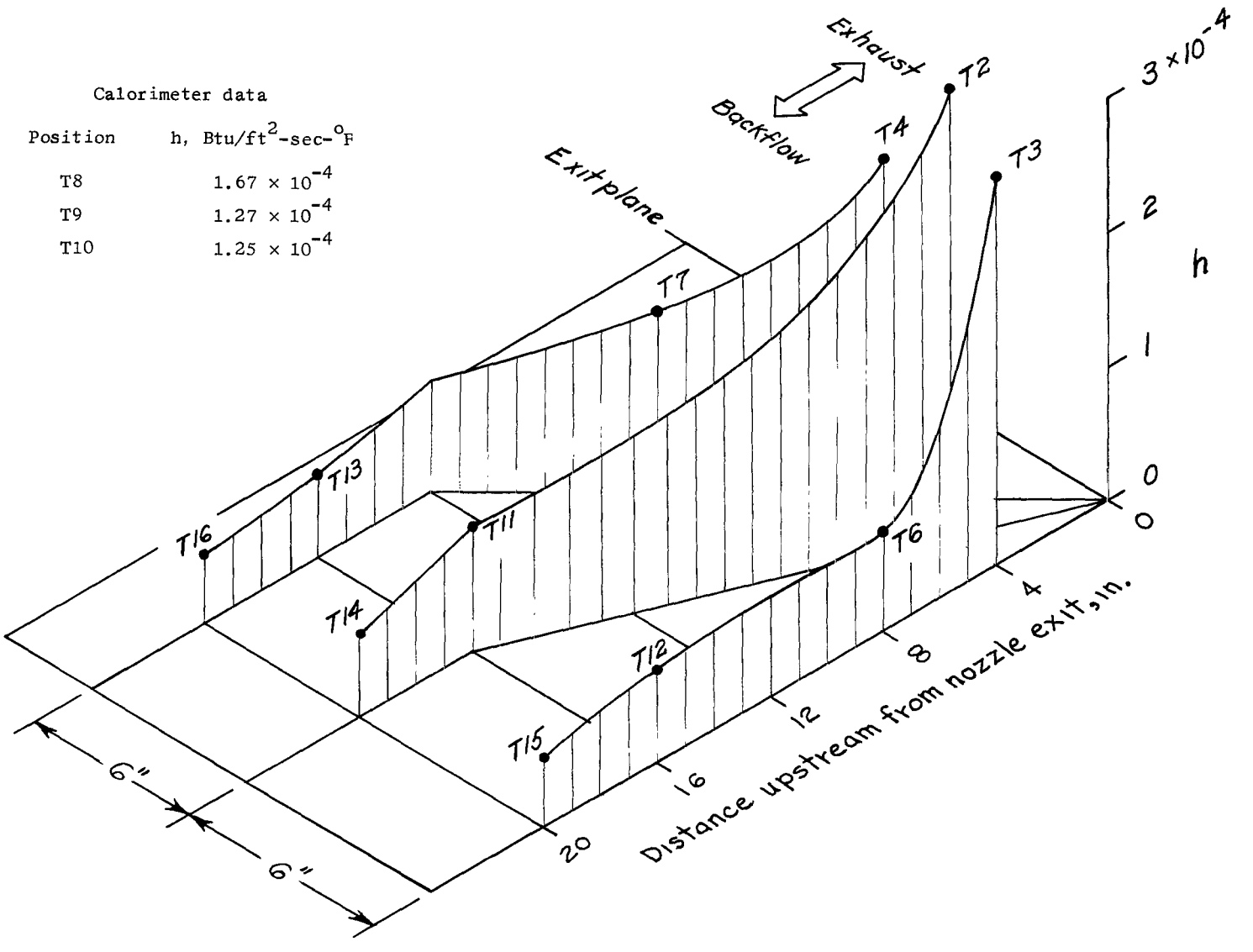

(a) Configuration I.

Figure 23.- Average heat-transfer-coefficient profiles obtained from thermocouples in backflow region.

Calorimeter data

Position	h, Btu/ft^2-sec-$^\circ$F
T8	1.02×10^{-4}
T9	0.36×10^{-4}
T10	0.44×10^{-4}

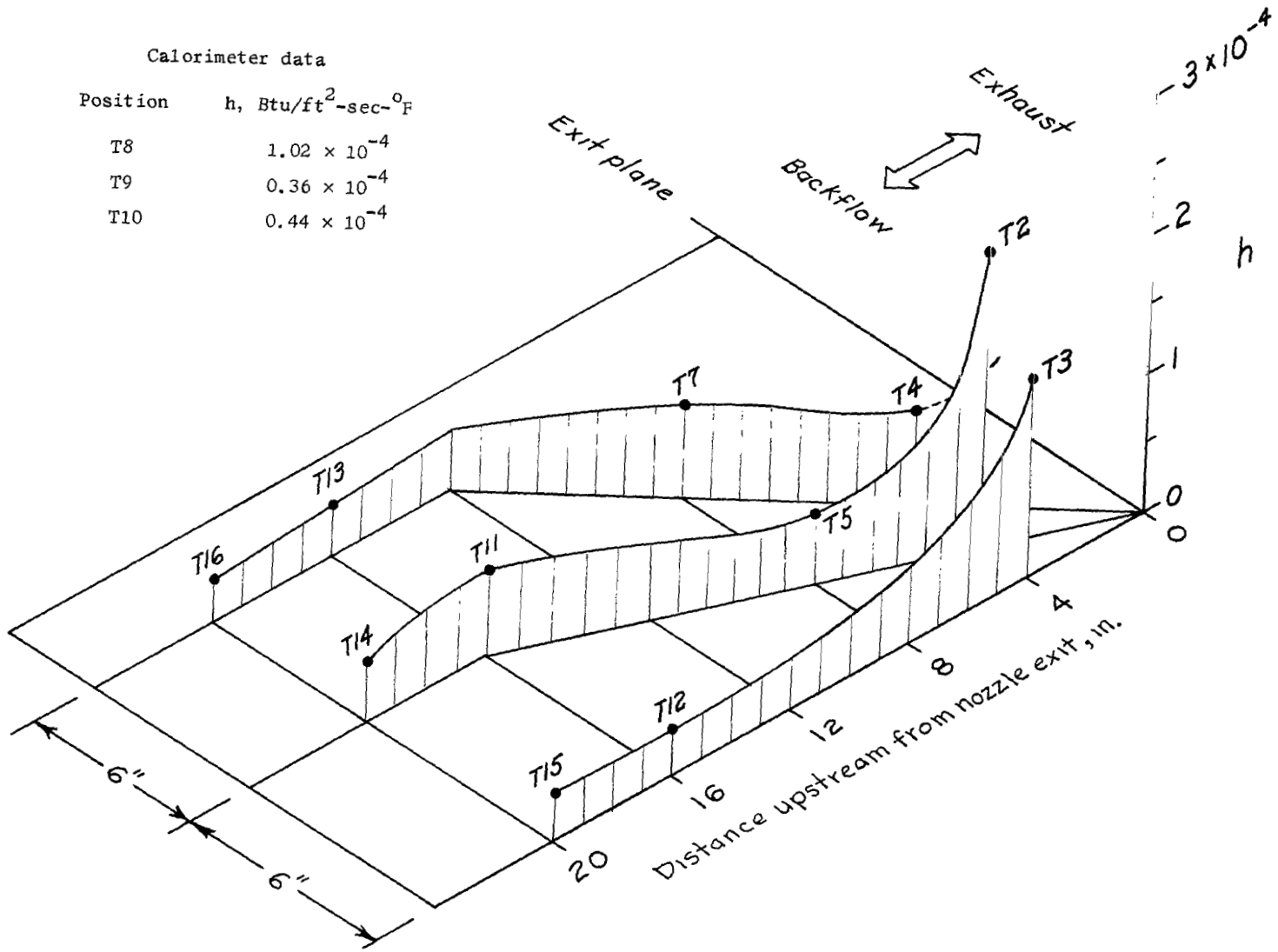

(b) Configuration II.

Figure 23.- Continued.

Calorimeter data

Position	h, Btu/ft^2-sec-$^\circ$F	
T2	1.74×10^{-4}	
T3	1.75×10^{-4}	
T5	2.99×10^{-4}	(perpendicular to backflow)
T10	0.66×10^{-4}	

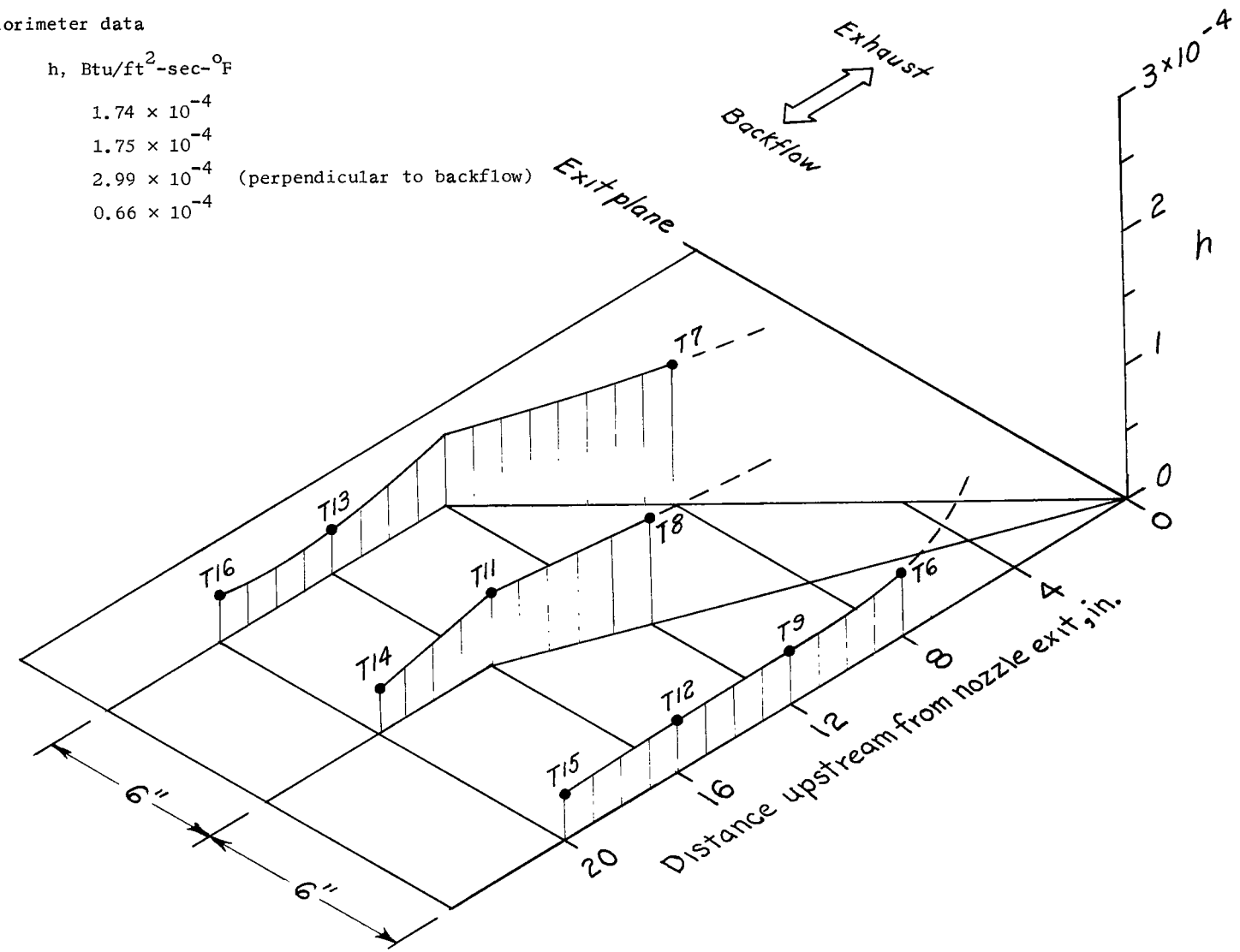

(c) Configuration III.

Figure 23.- Continued.

Calorimeter data

Position	h, Btu/ft^2-sec-$^\circ$F	
T2	3.15×10^{-4}	
T3	2.92×10^{-4}	
T5	2.65×10^{-4}	(perpendicular to backflow)
T10	0.88×10^{-4}	

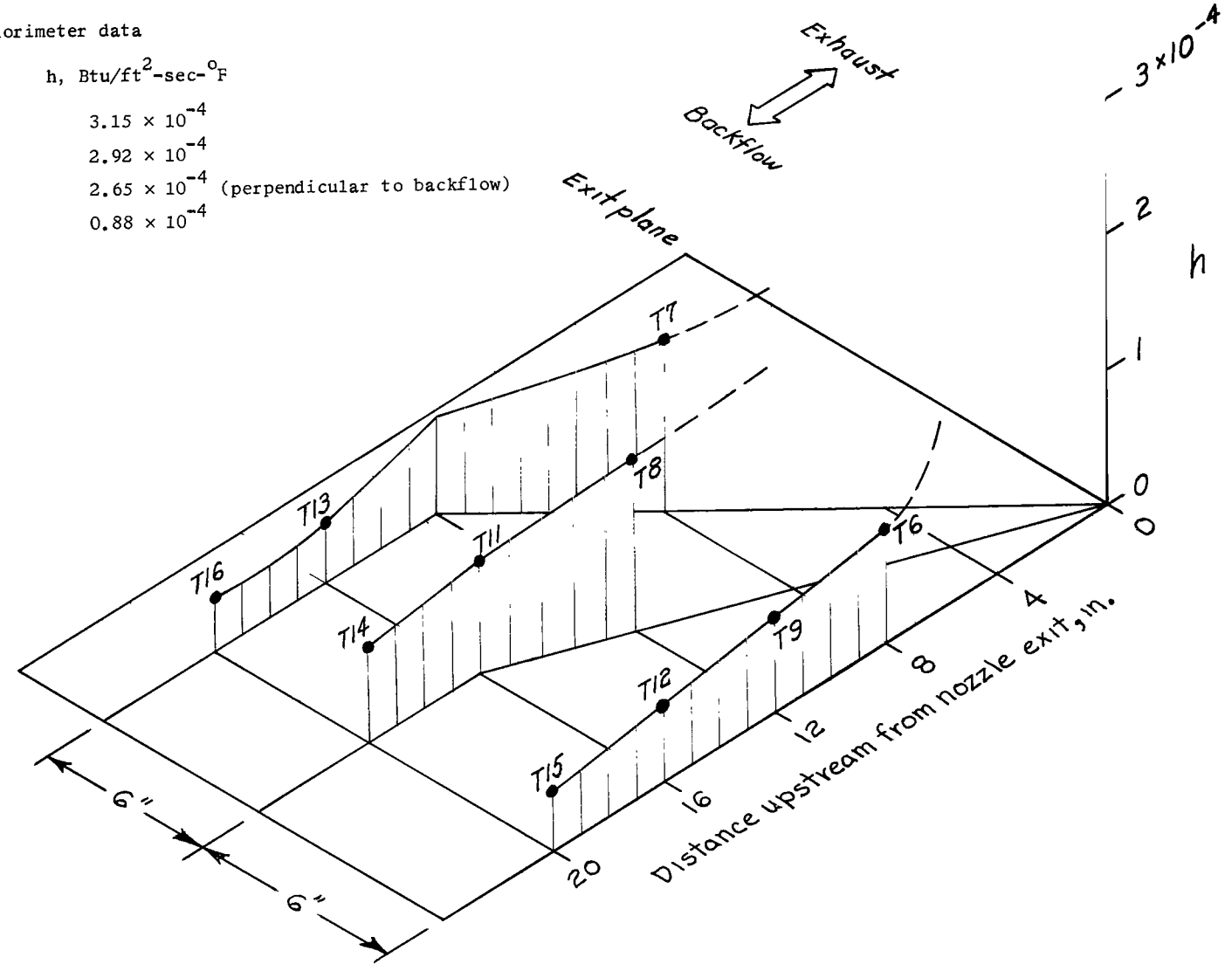

(d) Configuration IV.

Figure 23.- Continued.

Calorimeter data

Position	h, Btu/ft^2-sec-$^\circ$F
T5	1.60×10^{-4}
T6	1.56×10^{-4}
T7	0.74×10^{-4}

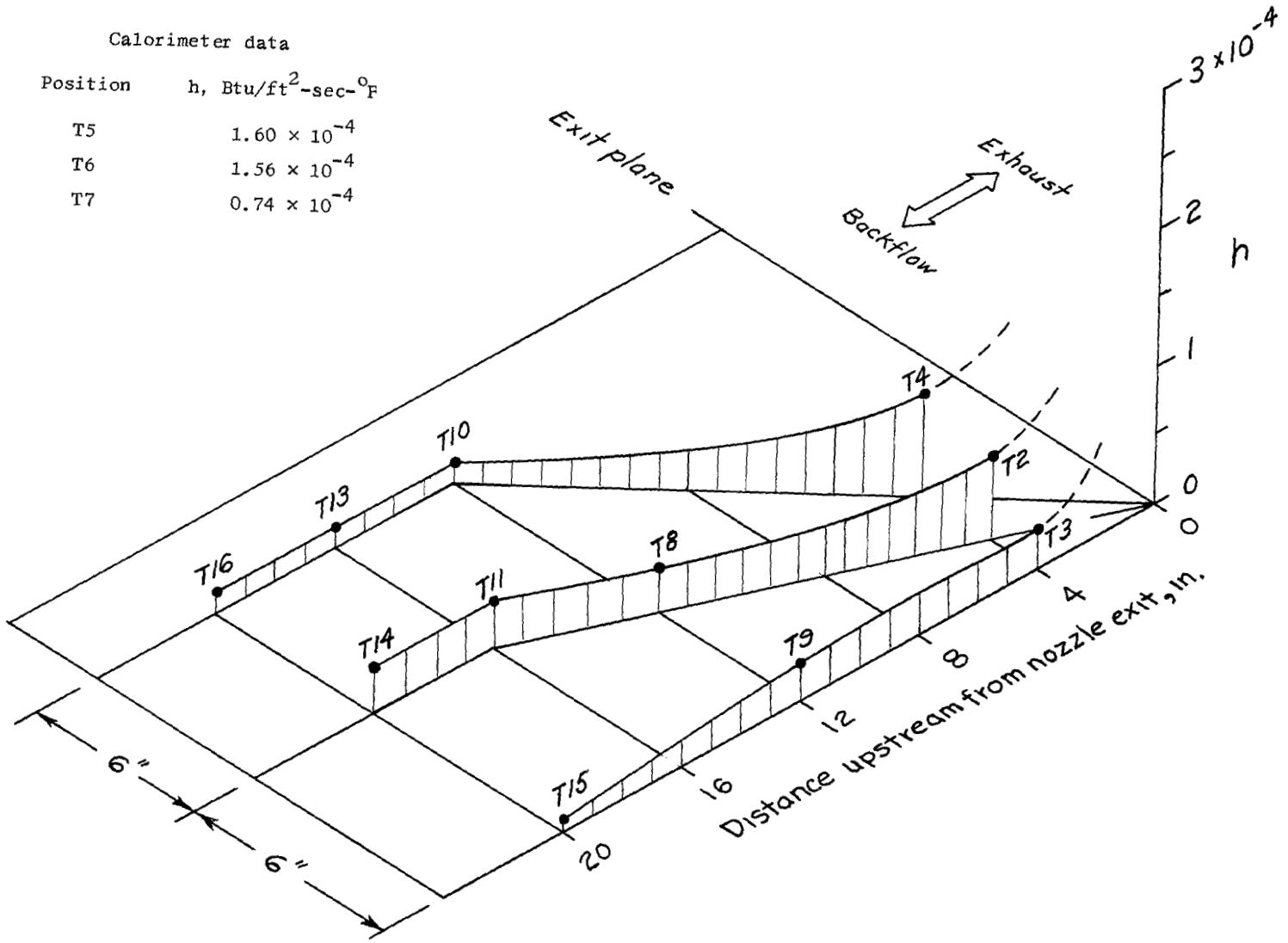

(e) Configuration V.

Figure 23.- Concluded.

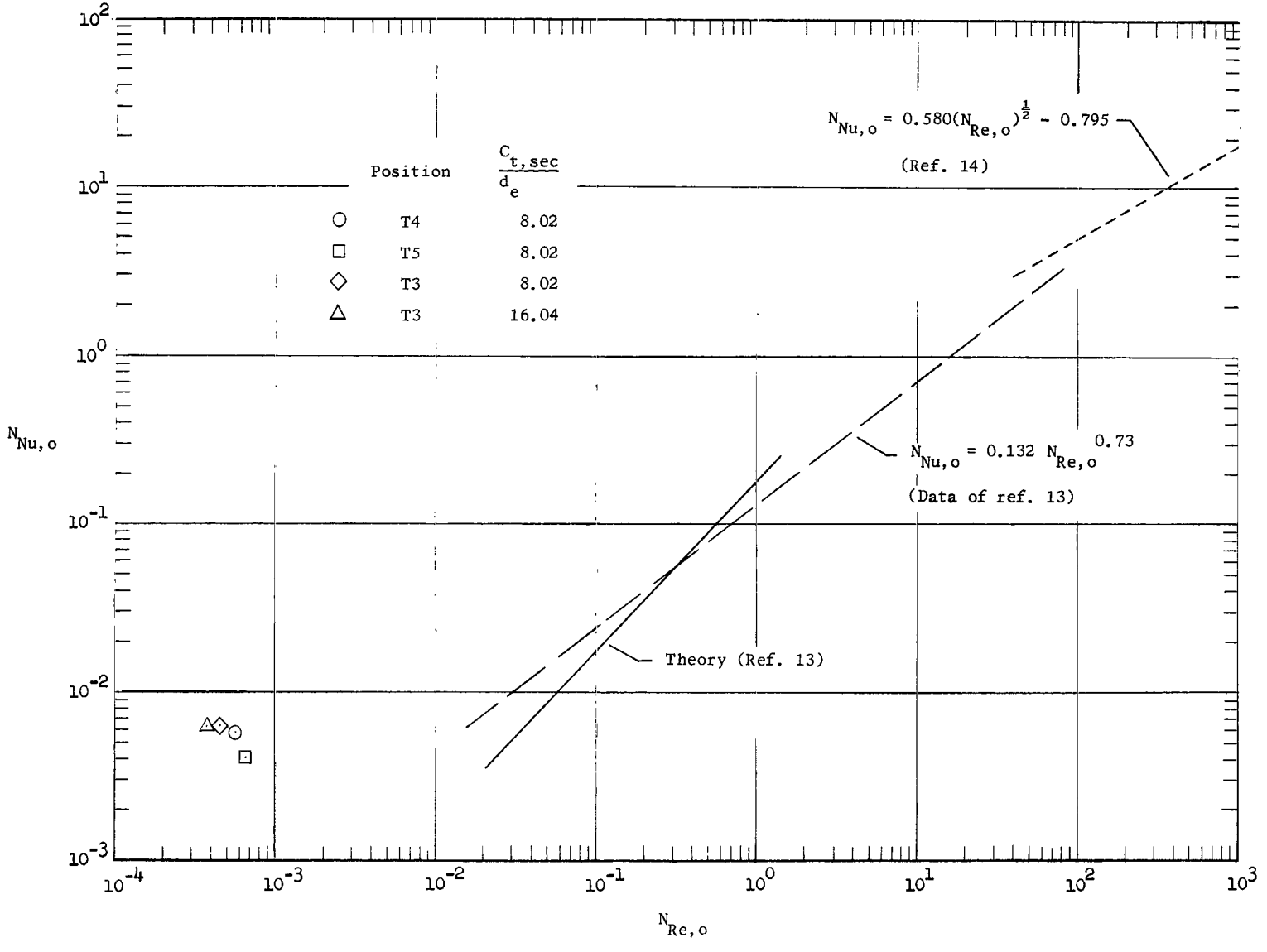

Figure 24.- Comparison of measured heat-transfer coefficients with theoretical and empirical values.

3/18/85

"The aeronautical and space activities of the United States shall be conducted so as to contribute . . . to the expansion of human knowledge of phenomena in the atmosphere and space. The Administration shall provide for the widest practicable and appropriate dissemination of information concerning its activities and the results thereof."

—NATIONAL AERONAUTICS AND SPACE ACT OF 1958

NASA SCIENTIFIC AND TECHNICAL PUBLICATIONS

TECHNICAL REPORTS: Scientific and technical information considered important, complete, and a lasting contribution to existing knowledge.

TECHNICAL NOTES: Information less broad in scope but nevertheless of importance as a contribution to existing knowledge.

TECHNICAL MEMORANDUMS: Information receiving limited distribution because of preliminary data, security classification, or other reasons.

CONTRACTOR REPORTS: Technical information generated in connection with a NASA contract or grant and released under NASA auspices.

TECHNICAL TRANSLATIONS: Information published in a foreign language considered to merit NASA distribution in English.

TECHNICAL REPRINTS: Information derived from NASA activities and initially published in the form of journal articles.

SPECIAL PUBLICATIONS: Information derived from or of value to NASA activities but not necessarily reporting the results of individual NASA-programmed scientific efforts. Publications include conference proceedings, monographs, data compilations, handbooks, sourcebooks, and special bibliographies.

Details on the availability of these publications may be obtained from:

SCIENTIFIC AND TECHNICAL INFORMATION DIVISION

NATIONAL AERONAUTICS AND SPACE ADMINISTRATION

Washington, D.C. 20546